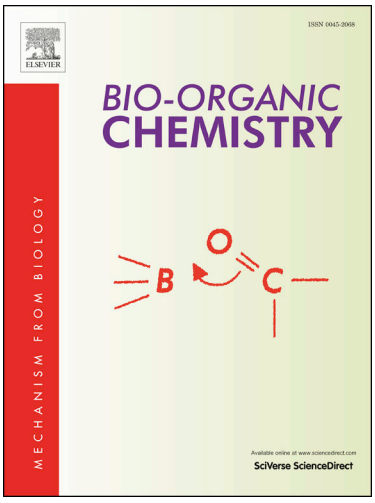

Synthesis, characterization and SAR studies of bis(imino)pyridines as antioxidants, acetylcholinesterase inhibitors and antimicrobial agents

Milena D. Milošević, Aleksandar D. Marinković, Predrag Petrović, Anita Klaus, Milica G. Nikolić, Nevena Ž. Prlainović, Ilija N. Cvijetić

PII: S0045-2068(20)31370-5
DOI: https://doi.org/10.1016/j.bioorg.2020.104073
Reference: YBIOO 104073

To appear in: *Bioorganic Chemistry*

Received Date: 13 January 2020
Revised Date: 2 May 2020
Accepted Date: 30 June 2020

Please cite this article as: M.D. Milošević, A.D. Marinković, P. Petrović, A. Klaus, M.G. Nikolić, N.Z. Prlainović, I.N. Cvijetić, Synthesis, characterization and SAR studies of bis(imino)pyridines as antioxidants, acetylcholinesterase inhibitors and antimicrobial agents, *Bioorganic Chemistry* (2020), doi: https://doi.org/10.1016/j.bioorg.2020.104073

Synthesis, characterization and SAR studies of bis(imino)pyridines as antioxidants, acetylcholinesterase inhibitors and antimicrobial agents

Milena D. Milošević[a], Aleksandar D. Marinković[b], Predrag Petrović[c], Anita Klaus[d], Milica G. Nikolić[e], Nevena Ž. Prlainović[b], Ilija N. Cvijetić[f,*]

[a]SI Institute of Chemistry, Technology and Metallurgy, National Institute, Department of Ecology and Techoeconomic, University of Belgrade, Njegoševa 12, 11000 Belgrade, Serbia

[b]Faculty of Technology and Metallurgy, University of Belgrade, Karnegijeva 4, 11000 Belgrade, Serbia

[c]Innovation Centre of Faculty of Technology and Metallurgy, University of Belgrade, Karnegijeva 4, 11000 Belgrade, Serbia

[d]Department for Industrial Microbiology, Institute for Food Technology and Biochemistry, University of Belgrade-Faculty of Agriculture, Nemanjina 6, 11080 Belgrade, Serbia

[e]Faculty of Sciences and Mathematics, Department of Chemistry, Višegradska 33, 18000 Niš, University of Niš

[f]Innovation Center of the Faculty of Chemistry, University of Belgrade, Studentski trg 12-16, 11000 Belgrade, Serbia

Abstract

In this study we synthesized a series of sixteen bis(imino)pyridines (BIPs) starting from 2,6-diaminopyridine and various aromatic aldehydes, and evaluated their antioxidant, antibacterial, antifungal and acetylcholinesterase (AChE) inhibitory activity. The chemical structures were elucidated by FTIR, elemental analysis, ESR and HRMS. ^{1}H and ^{13}C NMR spectra couldn't be acquired due to the formation of stable, carbon-centered radical cations in a solution, as confirmed by ESR spectroscopy and DFT calculations. The *in vitro* antioxidant potency was evaluated using four assays: free radical scavenging activity (DPPH and ABTS), reducing power and total antioxidant capacity assay. BIPs demonstrated excellent antioxidant properties, and two derivatives proved to be more potent than reference antioxidants (ascorbic acid and Trolox) in all assays. DFT calculations on ωB97XD/6-311++g(d,p) level of theory provided valuable insights into the radical scavenging mechanism of BIPs. For hydroxyl-substituted BIPs, hydrogen atom transfer (HAT) is a predominant mechanism, while the single electron transfer coupled with proton transfer (SET-PT) governs the antioxidant activity of other derivatives. Intramolecular hydrogen bonding (IHB) plays an important role in the mechanism of antioxidant activity as revealed by noncovalent interaction analysis and rotational barrier calculations. The spin density of radical cations is localized on carbon atoms

* Corresponding author; e-mail: ilija@chem.bg.ac.rs, Phone: +381 11 3336788

of a pyridine ring, which corroborates with *g*-factors and multiplicity obtained from ESR analysis. The most potent BIP exhibited moderate inhibitory activity toward AChE (IC_{50} = 20±4 μM), while molecular docking suggested binding at the peripheral anionic site of AChE with the MMFF94 binding enthalpy of –43.4 kcal/mol. Moderate *in vitro* antimicrobial activity of BIPs have been determined against several pathogenic bacterial strains: *Pseudomonas aeruginosa*, *Escherichia coli, Enterococcus faecalis*, *Staphylococcus aureus* and clinical isolate of methicillin resistant *S. aureus* (MRSA). The antifungal activity of BIPs toward *Candida albicans* was also confirmed. The similarity ensemble approach combined with molecular docking suggested leucyl aminopeptidase as the probable antimicrobial target for the three most potent BIP derivatives.

Keywords: Bis(imino)pyridines; Antioxidant activity; Density functional theory; Electron spin resonance; Antimicrobial activity; Acetylcholinesterase inhibition

1. Introduction

Currently, about 57% of approved drugs contain at least one heterocycle [1]. Among nitrogen-containing heterocycles, pyridine and its derivatives are very interesting compounds for biological, pharmacological and agricultural applications [2–5]. Particularly, bis(imino)pyridine derivatives (BIPs) represent a versatile class of compounds with antioxidant, antimicrobial, and antiproliferative activities [6,7]. BIPs as tridentate ligands are often utilized for the synthesis of organometallic compounds with a broad range of applications [7–9]. Schiff bases structurally similar to BIPs exhibited antimicrobial activity, and were more potent upon complexation to transition metal ions [7,10,11]. The presence of imino group appears to be essential for metal complexation and biological activity of BIPs. Also, pyrrole and thiophene-substituted heterocyclic Schiff bases are reported as highly potent, non-toxic antioxidants [12].

Aside from the broad spectrum of biological activities, BIPs are important compounds for many technological applications. They are utilized as polymer materials, corrosion inhibitors, catalysts for many organic reactions, analytical reagents and fluorescent sensors [13–15]. For example, *N,N′*-(pyridine-2,6-diyl)bis[1-(2-hidroxyphenyl)]methanimine (compound **6,** Fig. 1) incorporated into PVC membrane acts as a sensor for selective determination of Pb^{2+} ions. The same compound is a useful material for the extraction and analytical determination of Cu^{2+} ions in a solution [15]. BIPs-based polymers were successfully applied for the immobilization of glucose oxidase (GOx) [13].

Antioxidants are compounds that interact with harmful free radicals in the body and prevent their deleterious effects on biomolecules, and the knowledge of their mechanism of action is a prerequisite for the design of more potent compounds [16]. The radical scavenging activity is one of the most important mechanisms of antioxidant activity of compounds. The reactive free radical abstracts the H atom from the antioxidant via three mechanisms: hydrogen atom transfer (HAT), single electron transfer followed by proton transfer (SET-PT), and sequential proton loss electron transfer (SPLET). The inhibition of Fenton reaction through metal chelation of Fe^{2+} is another important antioxidant mechanism [17].

In HAT, a hydrogen atom (which can be observed as proton + one electron) is transferred from the antioxidant (Mol–H) to the free radical:

$$\text{Mol–H} \longrightarrow \text{Mol}^{\cdot} + \text{H}^{\cdot}$$

The HAT mechanism is quantified by the bond dissociation enthalpy, BDE:

$$\text{BDE} = H(\text{Mol}^{\cdot}) + H(\text{H}^{\cdot}) - H(\text{Mol–H}) \quad (1)$$

The stabilization of radical formed ($\text{Mol}^{\cdot}$) through the electronic and resonance effect lowers BDE values and contributes to the increased antioxidant activity of a molecule.

The SET-PT mechanism is initiated by the electron transfer (ET) from the antioxidant to the free radical, followed by deprotonation of radical-cation formed:

$$\text{Mol–H} \longrightarrow \text{Mol–H}^{\cdot+} + e^{-}$$

$$\text{Mol–H}^{\cdot+} \longrightarrow \text{Mol}^{\cdot} + \text{H}^{+}$$

The first step of this mechanism, SET-PT, determines the overall thermodynamic feasibility of this process and can be quantified by ionization potential, IP:

$$\text{IP} = H(\text{Mol–H}^{\cdot+}) + H(e^{-}) - H(\text{Mol–H}) \quad (2)$$

The higher is the stability of radical cation, the lower is IP values and SET-PT is a more feasible process. The second step, proton-transfer step, is characterized by proton dissociation enthalpy, PDE:

$$\text{PDE} = H(\text{Mol}^{\cdot}) + H(\text{H}^{+}) - H(\text{Mol–H}^{\cdot+}) \quad (3)$$

The SPLET mechanism starts with the deprotonation of the group responsible for antioxidant activity, followed by the ET from the anion:

$$\text{Mol–H} \longrightarrow \text{Mol}^{-} + \text{H}^{+}$$

$$\text{Mol}^{-} \longrightarrow \text{Mol}^{\cdot} + e^{-}$$

The first step of this mechanism is characterized by proton affinity, PA:

$$\text{PA} = H(\text{Mol}^{-}) + H(\text{H}^{+}) - H(\text{Mol–H}) \quad (4)$$

The ET step of this process is quantified by the electron transfer enthalpy, ETE:

$$\text{ETE} = H(\text{Mol}^{\cdot}) + H(\text{e}^{-}) - \text{H}(\text{Mol}^{-}) \quad (5)$$

In the Equations (1)-(5), enthalpies (*H*) of the molecule, radical, H atom, radical cation, anion, proton and electron are labeled as Mol–H, $Mol^{\cdot}$, $H^{\cdot}$, $Mol–H^{\cdot+}$, Mol^{-}, H^{+}, and e^{-}, respectively.

It should be noted that the net result of all three processes is the same, the transfer of H atom from antioxidant to free radical. The SET-PT and SPLET mechanisms involve charged intermediates which are better stabilized in polar media, so these are the preferred radical scavenging mechanism in polar environments.

Previous DFT studies on the antioxidant activity of phenolic Schiff bases revealed the importance of BDE for the rationalization of antioxidant mechanism but also showed that SET-PT is the main antioxidant mechanism of this type of compounds [6].

Our previous work on bis(styryl)pyridines revealed their moderate antioxidant capacities [18]. In the present study, we combined the benefits of pyridine moiety with two imine fragments to develop more potent bis-substituted pyridine antioxidants. As current literature lacks thorough studies on the antioxidant and antimicrobial activity of BIPs, herein we report the synthesis of 16 BIPs and SAR study of their antioxidant and antimicrobial activities. The structural characterization of BIPs using NMR spectroscopy was not possible due to the formation of a stable, paramagnetic species in a solution that caused broadening/disappearance of resonance signals. This difficulty is a possible reason for a limited number of studies on BIPs in the literature. The antioxidant potential of BIPs was mapped using different *in vitro* assays: DPPH, ABTS, CUPRAC and TAC (phosphomolybdenum method), and the underlying mechanisms were rationalized with the aid of DFT calculations. Antimicrobial activity of BIPs was determined toward three Gramm-positive and two Gramm-negative bacteria, and the plausible molecular targets for the most potent compounds were identified using molecular similarity approach and molecular docking. Also, AChE inhibitory potential of BIPs was determined and the results were supported by docking calculations.

2. Experimental

2.1. Materials and characterization methods

Full details on materials and characterization methods are given in Electronic Supplementary Information (ESI).

*2.2. Synthesis and characterization of symmetrical N,N'-(pyridine-2,6-diyl)bis[1-(substituted phenyl)]methanimine BIPs (**1-16**)*

The solution of substituted aromatic aldehyde (21 mmol) in 50 mL ethanol (Procedure A, applied for the synthesis of compounds **1, 2, 3, 6, 12** and **16,** Fig. 1) or 20 mL DMSO (Procedure B, applied for all other compounds) was added dropwise into a solution of 2,6-diaminopyridine (10 mmol) in 100 mL ethanol. The mixture was heated at 80°C for 2^{h} under N_2 atmosphere. The extent of reaction was monitored by TLC. Upon completion of a reaction, the precipitate was separated from the hot solution by vacuum filtration, washed with cold absolute ethanol and air-dried (Procedure A) or dried under N_2 (Procedure B).

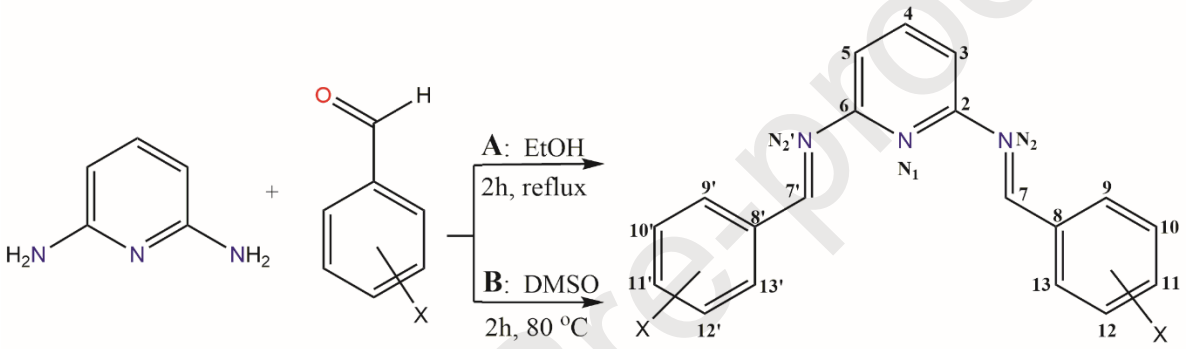

Compound	X[a]	Compound	X[a]
1	H	**9**	2-Qu [b,c]
2	1-naphthyl[b,c]	**10**	8-OH-2-Qu[b,c]
3	4-CH_3	**11**	4-Cl
4	4-OCH_3	**12**	4-F
5	3,4,5-tri-OCH_3	**13**	4-Br
6	2-OH	**14**	4-*N*,*N*(CH_3)$_2$
7	3-OH	**15**	4-NO_2
8	4-OH	**16**	2-Py[b,c]

[a] Numbering related to the aldehyde;[b] Numbering for compounds **2, 9, 10** and **16** are given in Fig.S1;[c] substituent X related to aldehyde residue.

Fig. 1. General procedure for the synthesis of BIPs (**1-16**)

Compounds **1**, **3** and **4** [19], **6** [20], **8** [19,21], **11** [19,22], **14** [13,19] have been previously synthesized as precursors and used *in situ* for the synthesis of other compounds. The detail characterization of previously reported BIPs using elemental analysis, melting point determination, IR and HRMS is given in ESI. The results showing the structure and purity of newly synthesized compounds are reported below. ESR spectra of compounds **8** and

14 are shown in ESI, Fig. S2. The atom numbering of synthesized compounds is outlined in Fig. 1.

N,N'-(pyridine-2,6-diyl)bis[1-(phenyl)]methanimine (**1**)

Yellow solid, yield 57%, m.p. >250 °C; Elemental analysis: Calcd. for $C_{19}H_{15}N_3$ (Mw = 285.35 g mol^{-1}): C, 79.98; H, 5.30; N, 14.73%; Found: C, 79.91; H, 5.36; N, 14.68%; IR, cm^{-1}: ν_{max}: 3377 brd (C-H stretching)$_{Py}$, 3057w, 3025w (C-H stretching)$_{Aryl}$, 2926s (C-H stretching)$_{Alkyl,}$ 1663sshp, (C=N stretching)$_{azomethine}$, 1578sshp (C=C stretching)$_{Aryl}$, 1445m (C=C asymmetric stretching)$_{Aryl}$, 1224w (C=N stretching)$_{Py}$, 1090m, 1027m (C-H in plane bending, 700shp (C-H out of plane deformation of phenyl group)$_{Aryl;}$ HRMS: calculated for $C_{19}H_{16}N_3$ $[M+H]^+$: 286.1347 observed: 286.1346.

N,N'-(pyridine-2,6-diyl)bis[1-(1-naphthyl)]methanimine (**2**)

Yellow solid, yield 55%, m.p. >270 °C, Elemental analysis: Calcd. for $C_{27}H_{19}N_3$ (Mw = 385.47 g mol^{-1}): C, 84.13; H, 4.97; N, 10.90%; Found: C, 84.05; H, 5.07; N, 11.00%; IR, cm^{-1}: ν_{max}: 3378brd (C-H)$_{Py}$, 3058w (C-H)$_{Aryl}$, 2926s (C-H)$_{Alkyl}$ 1600sshp (C=N)$_{azomethine}$, 1584sshp (C=C)$_{Aryl}$, 1477w (C=C)$_{Aryl}$, 1216w (C=N)$_{Py}$, 1022m (C-H)$_{Aryl}$, 770 (C-H)$_{Aryl;}$ HRMS: calculated for $C_{27}H_{20}N_3$ $[M+H]^+$: 386.1678 observed: 386.1680.

N,N'-(pyridine-2,6-diyl)bis[1-(4-methylphenyl)]methanimine (**3**)

Yellow solid, yield 42%, m.p. >280 °C, Elemental analysis: Calcd. for $C_{21}H_{19}N_3$ (Mw = 313.40 g mol^{-1}): C, 80.48; H, 6.11; N, 13.41%; Found: C, 80.35; H, 6.03; N, 13.52%; %; IR, cm^{-1}: ν_{max}: 3379 brd (C-H)$_{Py}$, 3020w (C-H)$_{Aryl}$, 2920s (C-H)$_{Alkyl}$, 2863shp (C-H stretching of CH_3)$_{Alkyl,}$ 1595sshp (C=N)$_{azomethine}$, 1509w (C=C)$_{Aryl}$, 1478w (C=C)$_{Aryl}$, 1222w, 1170w (C=N)$_{Py}$, 1020m (C-H)$_{Aryl}$ 778sshp (C-H)$_{Aryl}$; HRMS: calculated for $C_{21}H_{20}N_3$ $[M+H]^+$: 314.1657 observed: 314.1657.

N,N'-(pyridine-2,6-diyl)bis[1-(4-methoxyphenyl)]methanimine (**4**)

Yellow solid, yield 70%, m.p. >270 °C, Elemental analysis: Calcd. for $C_{21}H_{19}N_3O_2$ (Mw = 345.40 g mol^{-1}): C, 73.03; H, 5.54; N, 12.17%; Found: C, 72.98; H, 5.58; N, 12.20%; IR, cm^{-1}: ν_{max}: 3377brd (C-H)$_{Py}$, 3065w, 3000w (C-H)$_{Aryl}$, 2932s (C-H)$_{Alkyl,}$ 2834m (C-H stretching of CH_3-O)$_{Alkyl}$, 1609sshp (C=N)$_{azomethine}$, 1508m (C=C)$_{Aryl}$, 1461m (C=C)$_{Aryl}$, 1247s (Ph-O stretching), 1172s (CH_3-O stretching)$_{Alkyl}$, 1110w (C=N)$_{Py}$, 1031m (C-H)$_{Aryl}$, 810 (C-H)$_{Aryl;}$ HRMS: calculated for $C_{21}H_{20}N_3O_2$ $[M+H]^+$: 346.1561 observed: 346.1559.

N,N'-(pyridine-2,6-diyl)bis[1-(3,4,5-methoxyphenyl)]methanimine (**5**)

Yellow solid; yield 48%, m.p. >250 °C, Elemental analysis: Calcd. for $C_{25}H_{27}N_3O_6$ (Mw = 465.51 g mol^{-1}): C, 64.51; H, 5.85; N, 9.03%; Found: C, 64.48; H, 5.90; N, 9.10%; IR, cm^{-1}: ν_{max}: 3371 brd $(C-H)_{Py}$, 3060w, 3000w $(C-H)_{Aryl}$, 2937s $(C-H)_{Alkyl}$, 2834m (C-H of CH_3-$O)_{Alkyl}$, 1599sshp $(C=N)_{azomethine}$, 1502m $(C=C)_{Aryl}$, 1462m $(C=C)_{Aryl}$, 1232s (Ph-O stretching), 1183s (CH_3-O stretching)$_{Alkyl,}$ 1125s $(C=N)_{Py}$ 1003m $(C-H)_{Aryl}$, 776 $(C-H)_{Aryl;}$ HRMS: calculated for $C_{25}H_{28}N_3O_6$ $[M+H]^+$: 466.1899 observed: 466.1901.

N,N'-(pyridine-2,6-diyl)bis[1-(3-hidroxyphenyl)]methanimine (**7**)

Yellow solid, yield 45%, m.p. >250 °C, Elemental analysis: Calcd. for $C_{19}H_{15}N_3O_2$ (Mw = 317.35 g mol^{-1}): C, 71.91; H, 4.76; N, 13.24%; Found: C,72.01; H, 4.68; N, 13.19%; IR, cm^{-1}: ν_{max}: 3425sbrd (O-H), 3362 brd $(C-H)_{Py}$, 3030w $(C-H)_{Aryl}$, 2927s $(C-H)_{Alkyl}$, 1595sshp $(C=N)_{azomethine}$, 1481m $(C=C)_{Aryl}$, 1478w $(C=C)_{Aryl}$, 1230s $(C=N)_{Py}$, 1147 (Ph-O stretching), 1000m $(C-H)_{Aryl}$, 781 $(C-H)_{Aryl;}$ HRMS: calculated for $C_{19}H_{16}N_3O_2$ $[M+H]^+$: 318.1287 observed: 318.11280.

N,N'-(pyridine-2,6-diyl)bis[1-(2-quinolinyl)]methanimine (**9**)

Yellow solid, yield 71%, m.p. >280 °C, Elemental analysis: Calcd. for $C_{25}H_{17}N_5$ (Mw = 387.45 g mol^{-1}): C, 77.50; H, 4.42; N, 18.08%; Found: C, 77.45; H, 4.48; N, 18.12%; IR, cm^{-1}: ν_{max}: 3379 brd $(C-H)_{Py}$, 3055w $(C-H)_{Aryl}$, 2927s $(C-H)_{Alkyl}$, 1597sshp $(C=N)_{azomethin}$, 1503m $(C=C)_{Aryl}$, 1478m $(C=C)_{Aryl}$, 1306m $(C=N$ streching$)_{Aryl}$, 1233m $(C=N)_{Py}$, 1043, 1023m $(C-H)_{Aryl}$, 780 $(C-H)_{Aryl;}$ HRMS: calculated for $C_{25}H_{18}N_5$ $[M+H]^+$: 388.1455 observed: 388.1456.

N,N'-(pyridine-2,6-diyl)bis[1-(8- hydroxy-2-quinolinyl)]methanimine (**10**)

Red solid, yield 68%, m.p. >280 °C, Elemental analysis: Calcd. for $C_{25}H_{17}N_5O_2$ (Mw = 419.14 g mol^{-1}): C, 71.59; H, 4.09; N, 16.70; %; Found: C, 71.52; H, 4.05; N, 16.77 %; IR, cm^{-1}: ν_{max}: 3425sbrd (O-H), 3387 brd $(C-H)_{Py}$, 3032w $(C-H)_{Aryl}$, 2927s $(C-H)_{Alkyl}$, 1596sshp $(C=N)_{azomethine}$, 1504m $(C=C)_{Aryl}$, 1478m $(C=C)_{Aryl}$, 1326m $(C=N)_{Aryl}$, 1238s, $(C=N)_{Py,}$ 1195wbrd (Ph-O), 1011m $(C-H)_{Aryl}$, 781 (C-H); HRMS: calculated for $C_{25}H_{18}N_5O_2$ $[M+H]^+$: 420.1402 observed: 420.1410.

N,N'-(pyridine-2,6-diyl)bis[1-(4-fluorophenyl)]methanimine (**12**)

Yellow solid, yield 78%, m.p. >275 °C, Elemental analysis: Calcd. for $C_{19}H_{13}F_2N_3$ (Mw = 321.33 g mol^{-1}): C, 71.02; H, 4.08; N, 13.08%; Found: C,70.94; H, 4.12; N, 13.11%; IR, cm^{-1}:

ν_{max}: 3388 brd $(C\text{-}H)_{Py}$, 3066w $(C\text{-}H)_{Aryl}$, 2923s $(C\text{-}H)_{Alkyl;}$ 1600sshp $(C{=}N)_{azomethine}$, 1506m $(C{=}C)_{Aryl}$, 1477m $(C{=}C)_{Aryl}$, 1227s $(C{=}N)_{Py}$, 1152s, (Ar-F stretching), 1014m $(C\text{-}H)_{Aryl}$, 768 $(C\text{-}H)_{Aryl;}$ HRMS: calculated for $C_{19}H_{14}F_2N_3$ $[M+H]^+$: 322.1156 observed: 322.1150.

N,N'-(pyridine-2,6-diyl)bis[1-(4-bromophenyl)]methanimine **(13)**

Yellow solid, yield 76%, m.p. >270 °C, Elemental analysis: Calcd. for $C_{19}H_{13}Br_2N_3$ (Mw = 443.14 g mol^{-1}): C, 51.50; H, 2.96; N, 9.48%; Found: C, 51.58; H, 3.01; N, 9.42%; IR, cm^{-1}: ν_{max}: 3378 brd $(C\text{-}H)_{Py}$, 3047w $(C\text{-}H)_{Aryl}$, 2924s $(C\text{-}H)_{Alkyl}$, 1590sshp $(C{=}N)_{azomethine}$, 1482m, $(C{=}C)_{Aryl}$, 1448w $(C{=}C)_{Aryl}$, 1227w $(C{=}N)_{Py}$, 1010m $(C\text{-}H)_{Aryl}$, 768 $(C\text{-}H)_{Aryl}$; HRMS: calculated for $C_{19}H_{14}Br_2N_3$ $[M+H]^+$: 444.7546 observed: 444.7545.

N,N'-(pyridine-2,6-diyl)bis[1-(4-nitrophenyl)]methanimine **(15)**

Orange solid, yield 49%, m.p. >275 °C, Elemental analysis: Calcd. for $C_{19}H_{13}N_5O_2$ (Mw = 375.34 g mol^{-1}): C, 60.80; H, 3.49; N, 18.66%; Found: C, 60.76; H, 3.51; N, 18.73%; IR, cm^{-1}: ν_{max}: 3362 brd $(C\text{-}H)_{Py}$, 3030w $(C\text{-}H)_{Aryl}$, 2927s $(C\text{-}H)_{Alkyl}$, 1597sshp $(C{=}N)_{azomethine}$, 1500m $(C{=}C)_{Aryl}$, 1478w $(C{=}C)_{Aryl}$, 1350 (N=O stretching), 1228s $(C{=}N)_{Py}$, 1023m $(C\text{-}H)_{Aryl}$, 829s $(C\text{-}H)_{Aryl}$.. HRMS: calculated for $C_{19}H_{14}N_5O_2$ $[M+H]^+$: 376.1019 observed: 376.1021.

N,N'-(pyridine-2,6-diyl)bis[1-(2-pyridinyl)]methanimine **(16)**

Yellow solid, yield 68%, m.p. >250 °C, Elemental analysis: Calcd. for $C_{17}H_{13}N_5$ (Mw = 287.33 g mol^{-1}): C, 71.06; H, 4.56; N, 24.37%; Found: C, 71.10; H, 4.61; N, 24.31%; IR, cm^{-1}: ν_{max}: 3372 brd $(C\text{-}H)_{Py}$, 3045w $(C\text{-}H)_{Aryl}$, 2927s $(C\text{-}H)_{Alkyl}$, 1614sshp $(C{=}N)_{azomethine}$, 1500m $(C{=}C)_{Aryl}$, 1478w $(C{=}C)_{Aryl}$, 1300m $(C{=}N)_{Aryl}$, 1240s $(C{=}N)_{Py}$, 1076, 1049m $(C\text{-}H)_{Aryl}$ 768s $(C\text{-}H)_{Aryl;}$ HRMS: calculated for $C_{17}H_{14}N_5$ $[M+H]^+$: 288.1315 observed: 288.1321.

2.3. Synthesis of other 2,6-bis(imino)pyridine derivatives

To better understand the antioxidant activity of BIPs, structurally similar compounds **17** [23], **18** [24], **19** [24,25], **20** [7] and **21** [26] were synthesized and their characterization is given in ESI (Fig. S3).

2.4. Computational methods

The previous study showed that BIPs predominantly exist in enolimine form in the solid state and solution, so geometry optimization of BIPs started from bis(imino) structure [20,27]. The structures of the possible conformations of compound **1** are shown in Fig. S4. Concerning

the geometrical isomerism around imine bonds, *s*-trans/*s*-trans isomer was taken as an initial geometry, as this isomer proved to be more stable than *s*-cis/*s*-cis in structurally related bis(styryl)pyridines [18,28].

The initial 3D structures were generated using MMFF94 force field [29]. The conformational search was done by systematic rotation of all flexible bonds with 15° increment, using AMMP program implemented in Vega ZZ 3.1.0 [30]. The lowest-energy conformer was submitted to full geometry optimization at ωB97XD/6-311++g(d,p) level in the gas phase. The vibrational analysis confirmed that all structures correspond to a minimum of PES (no imaginary frequency). The solvent effects were accounted using the SMD model of water as a biologically relevant medium, methanol, and benzene whose low dielectric constant imitates the inner part of phospholipid membrane [31]. The solution enthalpies were obtained by adding the gas-phase thermal corrections to enthalpy (TCE) to the single-point energies calculated with the SMD model. This approach is justified by the fact that TCE does not significantly depend on a solvent model applied, while calculations of TCE with implicit solvation models extremely increase the computational time without giving an additional accuracy [32]. The geometry optimization of anions, radicals, and radical-cations was performed using the same procedure, where unrestricted calculations were performed for radicals and radical-cations. The solution enthalpies of H^+ and e^- were taken from [33], while enthalpy of H atom was calculated at the same level of theory.

For studying the intramolecular hydrogen bonding, bond critical points (BCPs) were calculated in Multiwfn 3.7 [34], starting from the geometries optimized at *ω*B97XD/6-311++g(d,p) level of theory. The noncovalent interactions (NCI) were visualized according to the method described in [35], implemented in Multiwfn program. NCI graphs were rendered in VMD [36]. The rotational barrier for **6** was calculated by scanning the dihedral angle between the phenol ring and azomethine moiety (C_7-C_8 bond). The reaction coordinate was systematically modified by 20° while all other geometry parameters were reoptimized. All calculations were performed using *ω*B97XD/6-311++g(d,p), in vaccum. Gaussian 16, revision B.01 was used for all DFT computations [37].

The structure of compound **16** was docked into the active site of AChE (PDB code 1Q83 [38]) using AutoDock Vina [39]. This structure is a protein-ligand complex with a large, bis-tacrine ligand which occupies both PAS and AS of AChE. Upon removal of ligand, the binding pocket remains in „open“ conformation that allows BIPs to reach all parts of AChE gorge. Exhaustiveness was set to 100 and 10 binding modes were calculated.

To identify the potential antimicrobial targets for BIPs, SMILES strings of all compounds were submitted to SEA Search Server [40]. 3D protein structure of leucyl-aminopeptidase identified in the previous step was retrieved from PDB code 1CP6 [41]. The ligand and water molecules were removed, hydrogen atoms were added to resemble protonation state at pH = 7.40 [42]. The protein structure was minimized using 100ps conjugate gradient minimization in NAMD 2.12 program [43] and CHARMM force field. The protein backbone was kept fixed to preserve the experimental structure, so only steric bumps were minimized. The active site was defined as all residues within a 12 Å radius from Zn^{2+} ion. AutoDock4Zn [44] parameters were used for docking in AutoDock 4.2, and VegaZZ 3.1.0 [30] and AutoDockTools 1.5.6 [45,46] were used for the preparation of input files. One pseudo atom was placed in tetrahedral orientation to Zn^{2+} ion where inhibitor should be coordinated. MMFF94 binding enthalpy calculation and binding mode visualization were done in LigandScout 4.2.6 [47].

2.5. Antioxidant capacity methods

All details about the methods for the determination of antioxidant capacity of BIPs are given in ESI.

2.6. AChE inhibition activity testing

The experimental procedure for the determination of AChE inhibition is given in ESI.

2.7. Antimicrobial activity testing

A detailed description of the methods for antimicrobial activity testing of BIPs is given in ESI.

3. Results and discussion

3.1. Synthesis and characterization

The compounds were synthesized by the condensation of 2,6-diaminopyridine with different phenyl-substituted aromatic aldehydes with the yields from 42 to 78% (Fig. 1). During the routine ^{1}H NMR analysis of the first three synthesized derivatives (**4**, **14**, and **15**), we were surprised by the absence of sharp resonance peaks. Even after the prolonged signal acquisition, only low-intensity, broad signals were obtained. Furthermore, we attempted to acquire NMR spectra of all other derivatives in three deuterated solvents ($CDCl_3$, DMSO-d_6,

and acetone-d_6) and using elevated temperature (50 ºC). Although the complete solubility of compounds (>10mg/0.4mL) was ensured, no peaks were obtained in any case (examples of NMR spectra of compounds **11** and **14** are given in ESI, Figs. S5 and S6). Nevertheless, there are studies reporting the successful characterization of BIPs using the NMR spectroscopy [48].

Therefore, we used different techniques to check the purity of the samples. According to elemental analysis, samples with a good purity were obtained directly from the reaction mixture by careful crystallization, washing with cold absolute ethanol and drying under nitrogen atmosphere. HRMS data further confirmed the purity of synthesized compounds (examples given in ESI, Figs. S7 and S8). Besides the molecular ion, M+1 and M+2 ions were observed. These ions can be attributed to partial or full reduction of azomethine group [49]. Interestingly, previously reported compound **10** was also obtained with high yield and purity without any purification [50]. Additionally, the characteristic IR absorption bands confirmed the presence of azomethine group, pyridine and aromatic rings.

Therefore, the confirmed BIPs purity and the observed absence of NMR signals suggest the presence of paramagnetic species in a solution. Although BIPs act as tridentate ligands, the synthetic method didn't include any metal ions as it was confirmed by analysis of the acidic extract from synthesized BIPs using inductively coupled plasma mass spectrometry (ICP-MS). Thus, the possibility for the formation of paramagnetic organometallic compounds in the course of BIPs synthesis was excluded. Searching for the possible explanations, we found one study reporting the inability to record NMR spectra of structurally similar BIPs [50]. Using the electron spin resonance (ESR) spectroscopy, the authors explained NMR-silence of BIPs through the formation of a stable, carbon-centered radical on a pyridine ring.

To test if this effect might explain the observed NMR silence, we recorded ESR spectra for all compounds. All tested compounds showed the same ESR pattern but with different intensities. The value of *g*-factor was about 2.006, indicating the formation of carbon-centered, not N-centered radicals for all compounds [50]. As a representative, the ESR spectra of **8** and **14** are given in ESI, Fig. S2. No hyperfine structure was observed in the ESR spectrum of any compound, indicating the absence of nuclei with nuclear spin 1 or ½ in the proximity of radical species. The results suggest the formation of a stable radical cation through the ionization of BIPs in a solution.

3.2. Antioxidant capacity of BIPs

The antioxidant capacity (AOC) of natural antioxidants is mainly associated with low-energy phenolic –OH bond(s), where highly stabilized radical species are formed after ET or HAT. Apart from four derivatives with –OH bonds, the structure of studied bis(imino)pyridines is very different from the structure of natural antioxidants. The AOC of sixteen BIPs was investigated using four *in vitro* assays mapping different antioxidant characteristics of a molecule: DPPH and ABTS as free radical methods, CUPRAC test as a measure of reducing capacity, and phosphomolybdenum assay characterizing the total antioxidant capacity of DIPs. The results obtained were compared with the AOC of two well-known standards, ascorbic acid and Trolox. Furthermore, DFT calculations were performed in order to gain more insights into the antioxidant mechanism of BIPs.

3.2.1. Free-radical methods

DPPH and ABTS tests have been widely used for screening the free radical scavenging ability of novel synthetic or natural products antioxidants. These measurements are based on the reduction of radical species through the electron- and/or hydrogen-atom transfer from antioxidants to the free radical which is accompanied by the change in absorbance.

It was previously shown that the heterocyclic imine-based Schiff bases possess a good antioxidant activity in DPPH and ABTS assays, where the presence of an electron-donating group on the phenolic ring improves the activity [12].

All sixteen BIPs showed good antiradical potency toward DPPH$^{\bullet}$, with IC_{50} values between 0.027 and 0.375 mM (Table 1). Compounds **8** and **10** were the most potent in DPPH assay, while **8**, **10** and **14** were the most potent antioxidants in ABTS test. The most potent compound **10** contains quinoline structure and hydroxyl group on heterocyclic moiety which might contribute to the extended π-electron delocalization and stabilization of radical species. The 8-hydroxyquinoline is recognized in the literature as a moiety with positive contribution to the antioxidant activity [51].

Additionally, within the subset of phenolic BIPs, the AOC is correlated with the position of the –OH group, with the following order of activity: **10**>>**8**>**7**>**6**. The presence of strong IHB in compound **6** is previously confirmed by crystal structure analysis [20], and this interaction makes hydrogen atom transfer to reactive radical species more difficult.

Table 1. The IC_{50} values for BIPs (**1-16**) determined in DPPH and ABTS free radical assays

Compound	DPPH IC_{50}*, mM	ABTS IC_{50}*, mM
1	0.280±0.051	0.120±0.024
2	0.289±0.040	0.111±0.007
3	0.153±0.022	0.178±0.011
4	0.168±0.025	0.084±0.035
5	0.184±0.033	0.140±0.057
6	0.175±0.021	0.195±0.009
7	0.109±0.005	0.088±0.018
8	0.084±0.045	0.034±0.014
9	0.215±0.015	0.117±0.023
10	0.027±0.010	0.031±0.011
11	0.184±0.022	0.218±0.012
12	0.197±0.014	0.191±0.022
13	0.162±0.016	0.209±0.016
14	0.188±0.031	0.030±0.011
15	0.375±0.020	0.247±0.051
16	0.226±0.037	0.205±0.022
Ascorbic acid	0.039±0.019	0.052±0.034

*IC_{50} values are expressed as mean ± standard deviation (SD) of three independent measurements

Compared to DPPH assay BIPs proved to be even more potent in ABTS test with the IC_{50} values range from 0.030 to 0.218 mM (Table 1). The results indicate that the positive contribution of electron-donating substituents is more pronounced than in DPPH test. For example, dimethylamino group as the strongest electron-donating substituent within this series yielded the most potent BIP derivative when introduced in *para*-position. The methoxy group, as another strong electron-donating substituent yielded a potent *para*-substituted derivative. The trend in the activity of hydroxyl derivatives is the same as for DPPH assay. Again, the least potent compound was *para*-nitro derivative (**15**), the strongest electron acceptor within this series.

3.2.2. Reducing power assay, total antioxidant capacity

The antioxidant activity of compounds is also attributed to the chelation of transition metal ions such as iron (Fe^{2+}) and copper (Cu^{+}) which have been proposed as catalysts for the *in vivo* formation of reactive oxygen species. Therefore, in addition to typical radical scavenging assays (DPPH and ABTS), reducing power method using CUPRAC have been applied to provide additional details about the AOC of BIPs. The good metal-chelating ability

of BIPs is already reported, acting as a good tridentate ligand forming pincer complexes with metal ions [52]. The results of CUPRAC assay were compared with Trolox as a reference antioxidant (Table 2) and determined from the ratio of molar absorptivity (ESI, Fig. S9, and Table S1). The compounds **10** and **14** bearing strong electron-donating groups had the highest AOC, while electron-withdrawing substituents (**11**-**13**, **15**) decreased the AOC.

Table 2. The results of CUPRAC assay, given relative to Trolox, and the results of total antioxidant capacity (TAC) assay using the phosphomolybdenum method, expressed as the equivalent mass of ascorbic acid.

	Reducing power assay	Total antioxidant capacity (TAC)
Compound	CUPRAC TEAC	Phosphomolybdenum assay
1	0.273	0.165
2	0.292	0.132
3	0.663	0.133
4	0.350	0.156
5	0.839	0.183
6	0.143	0.178
7	0.198	0.119
8	0.451	0.146
9	0.453	0.536
10	1.104	0.209
11	0.193	0.163
12	0.256	0.148
13	0.171	0.139
14	0.977	0.306
15	0.202	0.146
16	0.533	0.211
Trolox	1.000	-

Total antioxidant capacity (TAC) was performed by phosphomolybdenum test, which is based on the reduction Mo(VI) to Mo(V) and monitoring of corresponding change in the absorbance [53]. The obtained results are presented as mass equivalents of ascorbic acid (Table 2). The most potent compound **9** bears 2-quinoline substituents, indicating the importance of additional coordinating N-atoms in the complexation of Mo(VI).

3.3. DFT studies of structure-antioxidant capacity relationships

Antioxidant activity of the molecule is a direct consequence of its structure, conformation and solvent properties. The structural features which stabilize the radical species formed upon electron or hydrogen atom transfer improve the antioxidant capacity of a molecule. Therefore, not only the presence of particular functional groups but also the overall molecular geometry of antioxidant should be considered when deriving structure-antioxidant relationships within the congeneric series of compounds.

The geometry optimization of a ground state of BIPs provided the important structural parameters for further structure-antioxidant capacity relationship studies. The optimized structures of **1-16** are presented in Fig. 2 and geometry data are given in ESI, Table S2. The shortest bonds between central pyridine ring and imino groups are found for the strong electron-donating substituents like *N*,*N*-dimethyl (compound **14**), indicating that the electronic effects can be transferred from substituents to the central pyridine moiety.

Considering the symmetry of compounds, a large degree of planarity could be expected. Therefore, the values of torsional angles between the central pyridine ring and imino "arm" groups are studied (Fig. 2). This torsion will strongly influence the degree of conjugation through the molecule, which might have implications for the antioxidant activity. The lowest torsion angle of 10.64^{o} and the most planar structure is for compound **6**, due to presence of OH group in *–ortho* position to imino group. Such an arrangement enables intramolecular hydrogen bonding (IHB) between hydroxyl hydrogen and imino nitrogen thus forming six-membered rings and stabilizing almost planar structure. Somewhat higher values of torsional angle, around 16^{o} for the compounds **2**, **9** and **10** are probably due to the presence of rigid fused rings. For all other compounds, the values range between 23 and 26^{o}.

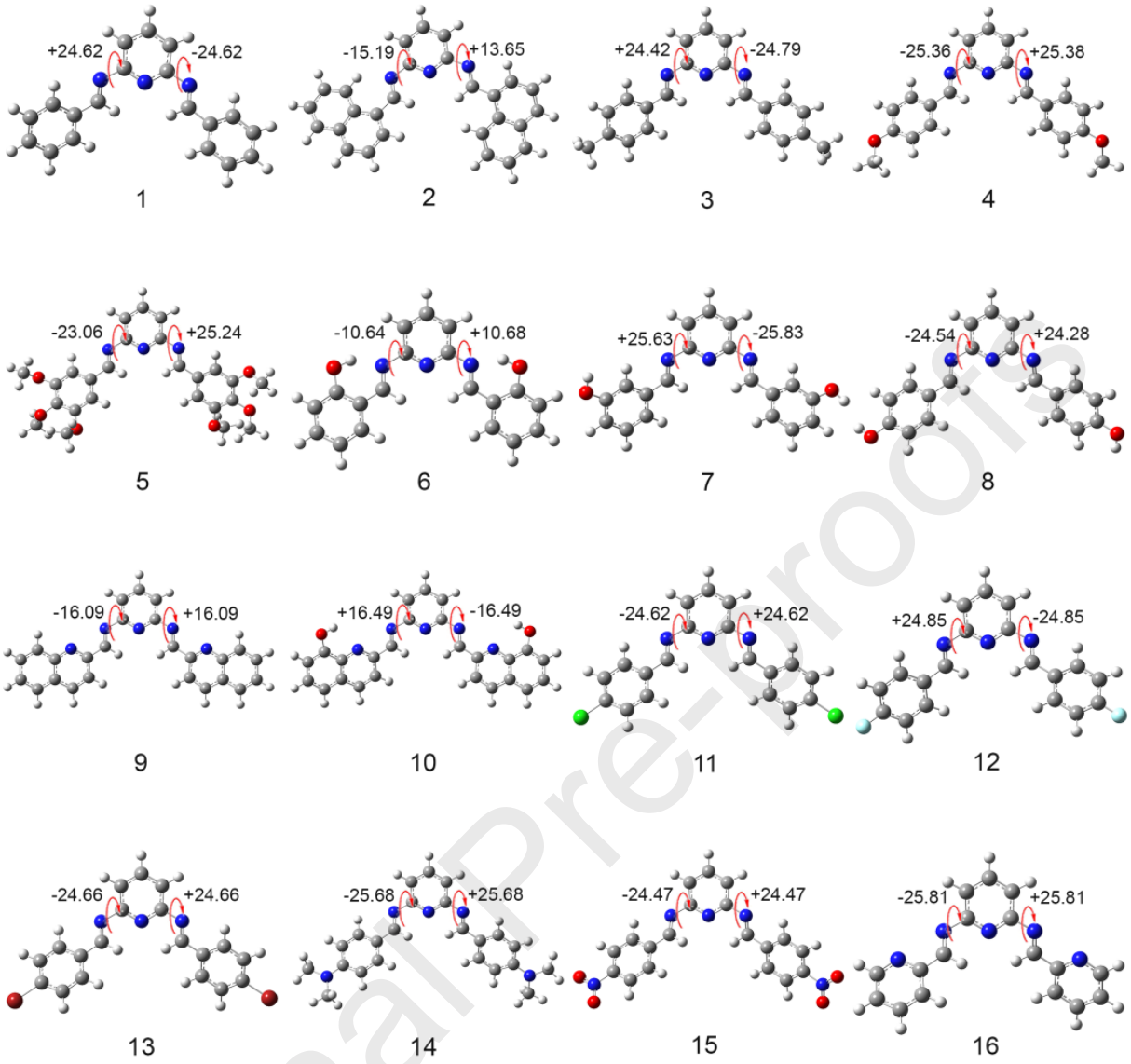

Fig. 2. Optimized geometries of BIPs with the torsional angles indicated

Molecules exhibit their antioxidant activity and diminish the oxidative stress by adopting one of the previously described mechanisms (HAT, SET-PT or SPLET), or their combination. According to the experimental data (Tables 1 and 2), it can be concluded that the electron-donating substituents improve, while electron-withdrawing substituents decrease the AOC of BIPs. To search for further details about the antioxidant mechanism of BIPs, we computed several molecular descriptors of the antioxidant activity using the DFT method in gas phase and simulating the solvation effects of water, benzene and methanol (Table 3).

Table 3. BDE, IP and PA values of BIPs computed at ωB97XD/6-311++g(d,p) level in the gas phase and using SMD solvation model of benzene, water, and methanol.

Comp.	Reactive group	BDE (kcal/mol)				IP (kcal/mol)				PA (kcal/mol)			
		Gas	C_6H_6	H_2O	MeOH	Gas	C_6H_6	H_2O	MeOH	Gas	C_6H_6	H_2O	MeOH
1	Imino	97.89	98.11	100.53	99.98	174.13	153.15	138.81	139.46	399.38	156.22	92.19	93.19
	Py 4-H	111.16	-	-		-	-	-	-	-	-	-	-
	Py 3-H	114.30	-	-		-	-	-	-	-	-	-	-
2	Imino	94.23	99.25	101.12	102.62	172.79	152.74	141.21	144.34	389.94	148.80	85.73	85.88
3	Imino	97.27	97.40	99.66	99.14	169.03	149.27	136.11	136.71	400.74	156.62	90.98	92.33
4	Imino	100.02	100.43	102.65	102.33	165.12	146.59	135.12	135.46	394.49	150.66	85.44	86.69
5	Imino	97.21	97.33	99.54	99.01	168.30	149.90	138.49	138.84	400.02	157.07	91.74	92.79
6	Imino	99.69	100.05	102.02	101.74	177.66	156.12	141.07	141.55	390.64	150.42	89.92	90.94
	OH	96.70	95.25	91.46	92.43	-	-	-	141.55	349.77	110.10	43.80	45.83
7	Imino	100.25	100.66	102.90	102.58	174.16	153.36	138.75	139.30	391.34	148.38	84.33	85.55
	OH	91.46	91.30	92.94	93.84	-	-	-	139.30	348.71	107.18	38.59	40.79
8	Imino	97.65	97.84	100.23	99.69	168.18	148.72	135.97	136.25	400.99	157.61	93.04	94.08
	OH	81.75	81.76	84.64	85.00	-	-	-	136.25	335.33	96.80	38.04	39.42
9	Imino	93.07	94.18	98.19	97.68	171.59	152.48	139.97	140.45	381.91	143.15	87.76	88.32
10	Imino	94.43	95.28	98.42	97.99	177.12	156.69	141.88	142.56	378.29	141.34	87.09	87.60
	OH	88.27	85.98	81.23	82.37	-	-	-	142.56	345.80	105.99	40.08	42.25
11	Imino	97.62	97.89	100.31	99.80	177.17	155.51	139.48	140.27	393.26	152.58	91.11	92.00
12	Imino	97.49	97.72	100.06	99.55	176.28	154.29	138.64	139.39	387.84	146.22	84.20	85.29
13	Imino	97.65	97.92	100.34	99.83	177.15	155.88	139.68	140.48	392.81	152.42	91.02	91.91
14	Imino	97.47	97.53	99.74	99.18	152.77	136.17	127.07	127.09	407.21	162.03	94.19	95.40
15	Imino	95.50	95.14	95.49	95.12	189.02	163.29	143.13	144.16	366.96	131.19	73.43	73.91
16	Imino	94.93	96.15	99.81	99.39	173.61	153.38	140.05	140.58	386.46	145.93	87.41	88.22

As a molecular descriptor of HAT, BDE was calculated for all compounds. Taking compound **1** as a model, we initially screened several hydrogen atoms (imino group and pyridine H-atoms) to find the lowest-energy bond. According to the results given in Table 3, the imino C–H atom is the most reactive site. Therefore, for all other BIPs the imino moiety was considered as HAT site. For hydroxyl-substituted derivatives **6**, **8** and **10**, the BDE of phenolic –OH group was also considered.

The thermodynamically feasible HAT reaction between DPPH$^{\bullet}$ and BIPs might be expected only for hydroxyl-substituted derivatives **8** and **10**, as BDE for DPPH$^{\bullet}$–H is 82.6 kcal/mol [54], so for all other compounds the equilibrium: BIP–H + DPPH$^{\bullet}$ $\rightleftharpoons$ BIP$^{\cdot}$ + $DPPH_2$ will be highly shifted toward reactants. The higher BDE values for **6** might be explained with the formation of IHB between the –OH group and imino N atom which stabilizes the ground state. The HAT from –OH group disrupts the IHB, leading to the larger energy difference between the ground state and O radical, and higher BDE according to Eq. (1).

To test the hypothesis that IHB plays an important role in the reaction of BIPs and DPPH$^{\bullet}$, we calculated the strength of IHB for two derivatives containing –OH group (**6** and **10**) using Atoms in Molecules (AIM) analysis. The positions of BCPs for IHB of **6** and **10** are indicated *via* NCI analysis, Fig. S10. Topology analysis provided several parameters such as electron density (ρ), Laplacian of electron density ($\nabla^2\rho$) and potential energy density (V(r)) which are correlated with the H-bond binding energy. According to Espinosa et. al [55], the strength of hydrogen bond (E_{HB}) can be approximated by 1/2 of V(r). The results are given in Table 4.

Table 4. Electron density, Laplacian of electron density, potential energy density, H-bond binding energy and donor-acceptor distance for O–H···N intramolecular hydrogen bonds of **6** and **10**.

Comp.	ρ, a.u.	$\nabla^2\rho$, a.u.	D-A distance, Å	V(r), a.u.	E_{HB}, kcal/mol
6	0.04772	0.1167	1.748	-0.04450	13.96
10	0.02466	0.0930	2.069	-0.01934	6.07

The nature of IHB in compound **6** is additionally studied by calculating the rotational barrier around the C_7-C_8 bond (Fig. S11). The calculated rotational barrier (15.52 kcal/mol) originates from strong IHB interaction with a small contribution of steric effect.

The exceptionally strong IHB of **6** rationalize its low antioxidant activity. On the other hand, compound **10** is a highly potent antioxidant in all assays (Tables 1 and 2) although IHB

might be expected in this structure as well. From Table 4 we can see that the strength of corresponding IHB is significantly lower compared to **6**, so hydroxy-group at position 8 is more available for the interaction with free radicals. Compared with the computed interaction energy for phenol-water pair (7.7 kcal/mol) [56], we conclude that –OH group of compound **6** remains „locked“ in pseudo 6-membered ring when solvated by explicit water molecules, while **10** prefers intermolecular H-bonding with solvent molecules, releasing the –OH group from intramolecular 5-membered ring.

The spin density (SD) distribution is a useful tool to visualize the degree of spin delocalization in the radical species formed upon HAT or SET-PT. Higher delocalization indicates better stabilization of radicals/radical cations, and lower BDE and IP values (Eqs. (1) and (2)). SD distribution maps can also provide information about the reactivity of various active sites in the molecule [57]. The SD distribution maps of two potent compounds **8** and **14** are shown in Fig. 3. Hydroxyl radicals (Fig. 3b) have much more pronounced spin delocalization compared to imino radicals (Fig. 3a). The spin density of radical cations (Figs. 3c and 3d) is delocalized over the entire molecule, where the majority of spin density is located at carbon atoms of the pyridine ring. The schematic representation of SD distribution for all 16 BIPs in the gas phase and water solvation model is given in ESI, Figs. S12-S15.

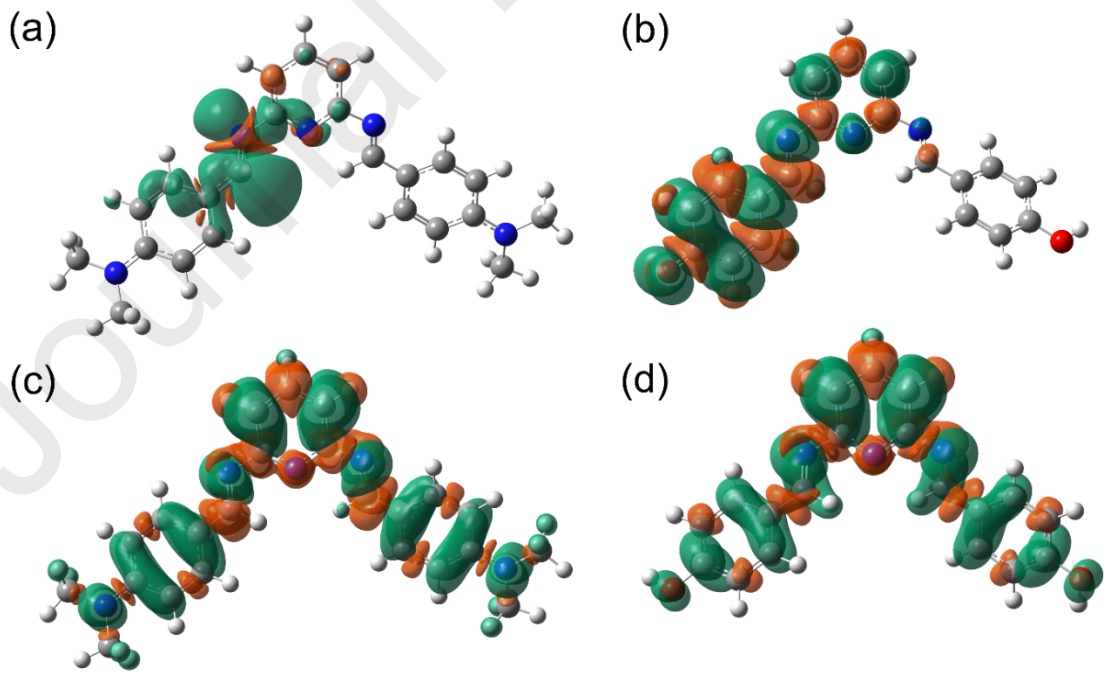

Fig. 3. Spin density distribution mapped for: (a) imino radical of **14**; (b) O radical of **8**; (c) radical cation of **14**; (d) radical cation of **8**, at the isovalue 0.0004 a.u.

Highly localized SD of imino radicals explains the weak influence of substituents on BDE values. On the other hand, pronounced delocalization of radical cation's SD indicate its stability and supports the presence of paramagnetic species in a solution. Overall results reveal weak dependence of BDEs on substituent's nature and the medium tested, so additional descriptors are necessary to fully rationalize the experimental results.

The suggested formation of stable radical cation in a solution indicates the facile ionization of BIPs, which should favor the SET-PT mechanism. The lowest value of IP in all environments is found for compound **14**, and the highest for compound **15**. As those compounds have strong electron-donating or electron-accepting group attached in *p*-position of benzene rings, respectively, this implies that the IP is strongly influenced by the position and nature of substituents. Furthermore, statistically significant correlations between IP and Hammett substituents constants (Fig. S16) suggest that the ionization potential of BIPs might be successfully predicted using LFER principles, thus saving computational time for the design of novel BIP-based antioxidants. On the other hand, the low statistical validity of BDE *versus* σ constant correlations (r = 0.02 (for gas phase) to 0.08 (for water)) was observed, which further confirms the weak influence of substituents on BDE of BIPs.

Accordingly, high BDE of compound **14** suggests that HAT is not a thermodynamically favorable process, so SET-PT mechanism must be an important contributor to the excellent potency of **14** observed in DPPH and ABTS tests.

From the thermodynamic point of view, the preferred antioxidant mechanism is determined by the absolute values of BDE, IP, and PA as the first step of HAT, SET-PT and SPLET mechanisms, respectively. From Table 3 it is clear that HAT is a favorable radical scavenging mechanism in the gas phase and benzene, while SPLET is feasible only in water. It should be noted that the overall antioxidant performance of a compound also depends on the nature of scavenged free radical, the explicit interactions with the environment, as well as the kinetics of the process.

There is another common procedure for the elucidation of a preferable antioxidant mechanism from the DFT-computed descriptors. According to Wright et al. [58], two main radical scavenging mechanisms, HAT and SET-PT, occur simultaneously but with different rates, and the dominant process can be elucidated from the difference in gas-phase BDE and IP between phenol and antioxidant. They concluded that the HAT dominates for antioxidants with ΔBDE $\approx$ –10 kcal/mol and ΔIP up to –36 kcal/mol, while SET-PT is a dominant mechanism for antioxidants with ΔIP above –45 kcal/mol. Taking into account the

experimental data for BDE and IP of phenol (88.0 kcal/mol and 196.2 kcal/mol, respectively) [58,59] and the data from Table 3, we conclude that HAT is a dominant mechanism for hydroxyl-substituted derivatives **8** and **10**, while SET-PT is a dominant mechanism for compound **14**.

The main mechanism for compound **8** (4-OH derivative) can be also deduced by the comparison with experimental data of 4-OCH_3 derivative (compound **4**). Compound **4** lacks the reactive –OH group and cannot react *via* HAT mechanism, while stronger electron-donating groups should additionally stabilize radical cation, favoring the SET-PT mechanism. Substitution of –OH with –OCH_3 group increases the IC_{50} values 2-3 times (Table 1), indicating that HAT is a dominant mechanism for compound **8**.

3.5. Structure-antioxidant capacity relationships - Interpretation of mechanisms by correlation methods

The antioxidant mechanism of the BIPs was also analyzed using one- and two-parameter linear regression analysis, *i.e.* linear free energy relationships (LFER) principles. Correlation analysis of DFT descriptors such as HOMO/LUMO energies, energy gap (E_{gap}) values (ESI, Table S3), BDE, and IP (Table 3), along with Hammett constants (ESI, Table S4) with the antioxidant activities further help in the interpretation of the antioxidant mechanisms.

The BIPs radical scavenging ability *versus* HOMO energy value (Table S3) was considered in the first step. The exponential and linear relations of DPPH and ABTS activity *versus* HOMO energy are given in Figs. S17 and S18, respectively. From Fig. S18, increased activity *versus* increasing HOMO energy was observed. Generally the electron-donating groups increase the energy of HOMO orbitals, while opposite trend is for electron-accepting groups. Also, E_{gap} values generally follow a similar trend (ESI, Fig. S19 and Table S3). For compound **10**, the appropriate stabilization of HOMO/LUMO orbital leads to the lowest E_{gap}. In this compound, both HOMO and LUMO orbitals are delocalized symmetrically over 8-hydroxyquinolin-2-yl moiety in former and imino moieties in later orbital. Also, IHB and electron-donating character of dimethylamino and hydroxy groups in compounds **6**, **8** and **14**, respectively, cause a higher extent of delocalization (Fig. S19), leading to the increased activity. The linear dependence of ABTS activity *versus* HOMO energy (Fig. S18) is in accordance with the proposed antioxidative mechanism (Eq. (2)).

The results obtained from preliminary correlations between IC_{50} and BDE, IP and PA, using all synthesized compounds, showed low statistical validity. Acceptable and similar correlation results of IC_{50} (DPPH and ABTS) and TEAC (CUPRAC) *versus* BDE were

obtained for the compounds **6** - **8** and **10** in water and methanol (ESI, Figs. S20, S22, and S24, respectively). Different type of correlation line was obtained: linear for DPPH assay (Fig S20), and parabolic for ABTS and CUPRAC (Figs. S22 and S24). Such results indicate that HAT is a favorable mechanism for hydroxy-substituted compounds **6**, **8** and **10** in DPPH assay, while in the ABTS and CUPRAC assays other processes also participate, with the main contribution of HAT process. Also, the different trends of the correlation lines of DPPH, ABTS and CUPRAC scavenging data *versus* IP for the other compounds, given in Figs. S21, S23 and S25, indicate a complex mechanism of antioxidative activity. In line with this, the opposite slopes of linear correlations, obtained for IC_{50} *versus* IP for ABTS (Fig. S23) and CUPRAC assay (Fig. S25) in two solvents, corroborate with the complex influences of different parameters on obtained AOC values.

The AOC of BIPs is also correlated with Hammett σ constants (Figures S26-S29). Different types of correlations are observed for DPPH, ABTS, CUPRAC and TAC activity *vs*. Hammett σ constants, suggesting that electronic effects of substituents are not solely responsible for the antioxidant mechanism of BIPs.

The LFER multi-parameter approach was valuable in an estimation of the contributions of thermodynamic values BDE and IP to the measured antioxidant activity. Thus, the obtained correlation results, with the assumption that correlation coefficients relate to contributions of HAT and SET-PT mechanism, were used in an analysis of the overall antioxidant mechanism. The two-parameter correlation approach using a set of obtained activities (Table 1) versus BDE and IP descriptors (Table 3) yielded the correlation results (Table S5) used for calculation of the percentage contribution of HAT and SET-PT mechanism (Table S5). The correlation results were used for the analysis of the nature of antioxidant mechanism for BIPs. Results from two-parameter correlations of IC_{50} *versus* BDE and IP, including all compounds, indicated a somewhat higher BDE contribution, 52%, over IP, 48%, in DPPH assay (Table S5). Exclusion of compound **15** from correlation increased the BDE contribution to 69%, while the opposite is true if dimethylamino is excluded (46%). This result indicates that dimethylamino group contributes to the significant stabilization of imino radical formed, *i.e.* stabilization of the benzylidene radical is strongly favored by the extended π-delocalization. Exclusion of all hydroxyl-substituted BIPs did not provide satisfactory correlations, while the exclusion of 4-OH substituted BIP decreased HAT contribution to 38% (Table S5). Different correlation results were obtained for ABTS test considering all compounds studied. A higher IP contribution of 65% suggests that the molecule reacts primarily with the $ABTS^{\bullet+}$ *via* SET-PT mechanism. Exclusion of compounds **1**, **2**, **4** and **9**

improved the statistical validity of correlation with 40% and 60% of HAT and SET-PT participation, respectively. The opposite correlation obtained by the exclusion of compounds **2**, **4**, **6-8** and **10**, indicates the prevalence of SET-PT mechanism in water and methanol. Ortho-hydroxy substituted compound **6** behaves as SET-PT promoting compound due to π-delocalization within pseudocyclic structure which prevents an efficient H atom abstraction (Fig. S10). In general, the obtained correlation results, summarized in Table S5, indicate that the radical scavenging mechanism is composed of the appropriate contribution of the electron (IP) and H atom (BDE) transfer steps, depending on electronic properties and the nature of substituents.

To find the additional evidence on the antioxidant mechanism of BIPs, compounds **17-21** (Fig. S3) were synthesized and tested in DPPH and ABTS assays. Consideration of the structural analogy and antioxidant activities helped in the understanding of active sites taking place in a concomitant process of electron and proton abstraction. Structural isomerism of compounds **1** and **17** and similar activity (12% and 20% higher activity of compound **17**) indicate on similar effect on stabilization of either radical or radical cation formed in DPPH and ABTS test, respectively. It could be supposed that participation of both HAT and SET-PT takes place in a DPPH assay, while SET-PT is a major process in ABTS assay. Also, the significant increase of DPPH activity for compound **18** (48% higher than for **6**) indicates the existence of a free hydroxyl group able to participate in the HAT process. This is opposite to the structurally arranged hydrogen bonding in compound **6** which decreases the effectiveness of hydrogen transfer. Fairly similar activity of compounds **8** and **19** (less than 10% difference) confirmed this conclusion. Additionally, increased and decreased DPPH activity of compounds **20** and **21** for 22% and 46%, respectively, compared to compound **1**, indicate that the HAT process participates at approximately 46% considering imino radical formation (Table S5). Otherwise, a similar activity of compounds **1** and **21** in ABTS test is additional evidence of the derived conclusions.

In summary, these results showed complex influences of structural and electronic effects of substituents on the HAT and SET-PT processes, which participate in the overall antioxidant mechanism in different extents depending on the assay performed.

3.6. AChE inhibitory activity of BIPs

All tested compounds showed poor to moderate inhibitory activity towards AChE (ESI, Fig. S30 and Table S6). The most potent derivative was compound **16** (IC_{50} = 21±4 μM) bearing two *o*-pyridyl substituents. The low potency of BIPs bearing various substituents with

different electronic and steric effects indicates that further modification of scaffold is necessary to achieve inhibitory activity in nanomolar range. To elucidate the binding mode of **16** into the active site of AChE, molecular docking was performed. The tentative binding mode and ligand interaction diagram are shown in Fig. 4.

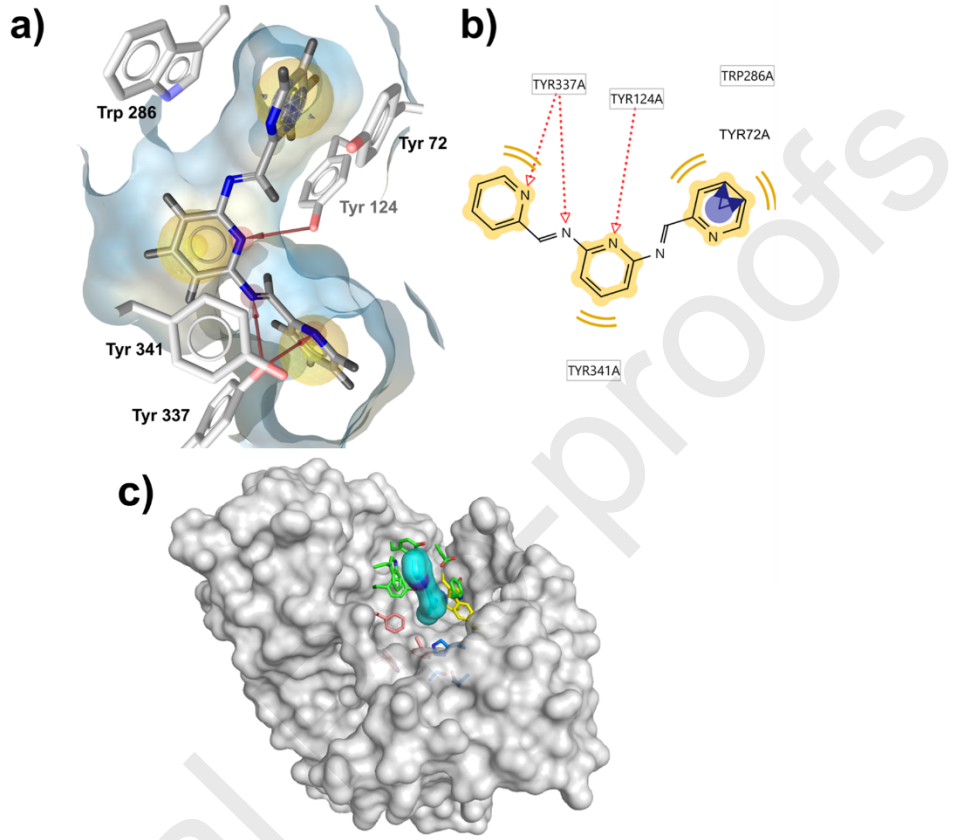

Fig. 4 a) Binding mode of **16** into the active site of AChE obtained by docking calculations. The hydrophobic pharmacophores are shown as a yellow sphere, and hydrogen-bond acceptor pharmacophores are shown as red spheres. Hydrogen bonding interactions between protein and ligand are depicted with red arrows while stacking interactions between **16** and Trp 286 and Tyr 72 are shown as blue rings on the upper pyridine ring of a ligand; b) Ligand interaction diagram showing a 2D depiction of stabilizing interactions between **16** and AChE; c) The orientation of **16** (light blue sphere) inside AChE binding pocket. Amino acid residues comprising peripheral anionic site are colored green, the acyl-binding pocket is in red, deep anionic site is in yellow, and catalytic triad (Glu 334, His 447, Ser 203) is shown as blue sticks.

As can be seen from Fig. 4c, compound **16** occupies mainly peripheral anionic site (PAS) located at the rim of AChE binding pocket [60]. One pyridyl substituent forms π- π stacking interactions with Trp 286 and Tyr 72, and central pyridine ring forms hydrogen bond with Tyr 124. The pyridine central ring also forms hydrophobic interactions with Tyr 341. The only interacting residue outside PAS is Tyr 337, a part of anionic site (AS) located deeper

in the AChE gorge. The calculated binding affinity was -8.9 kcal/mol, and MMFF94 binding enthalpy was -43.43 kcal/mol. An increase in the molecular size to allow more interactions inside AS, particularly with Trp 86, appears as a rational structural modification to improve the potency of BIPs toward AChE.

3.7. Antibacterial and antifungal activity of BIPs

BIPs and particularly their metal complexes are often studied as antimicrobial agents [7,24]. To evaluate the antimicrobial potential of **16** BIPs and derive preliminary SAR information, we tested all compounds toward several Gramm + and Gramm – strains that are common human pathogens, as well as one fungus (*C. Albicans*). Screening the several bacterial and one fungal strain we aimed to gain more general insights into the antimicrobial potential of BIPs.

The tested compounds showed bacteriostatic potential toward all studied bacteria (Table 5). The compounds were very effective against *E. coli* (MIC 0.31 - 5.00 mmol/L), *E. faecalis* (MIC 0.16 - 5.00 mmol/L) and *S. aureus* (MIC 0.16 - 5.00 mmol/L). More importantly, the compounds were active against highly resistant *S. aureus* MRSA (MIC 0.08 - 5.00 mmol/L). Along with this, almost half of the analyzed compounds exert a fungistatic effect toward *C. albicans* (MIC 0.16 - 5.00 mmol/L). The compound **16** showed the ability to destroy the bacteria *E. faecalis* and *P. aeruginosa* (MBC 5.00 mmol/L).

Previous studies have shown that compounds **6**, **8** and **16** exert moderate antimicrobial activity while metal complexation significantly improves the activity [7]. Two compounds, **16** and **6**, exerted a potent fungicidal effect against *C. albicans* comparable with fluconasole (MBC 0.31 mmol/L for **16** vs. 0.16 mmol/L for fluconasole). The overall assessment indicated that among sixteen studied BIPs, compound **16** (bis-2-pyridyl derivative) was the most potent antimicrobial agent, followed by 2-OH derivative (compound **6**).

Table 5. Antimicrobial activity of BIPs, amoxicillin (AMX, used only for bacterial strains) and fluconazole (FLU, used only for fungal strain), expressed as MIC (mmol/L) and MBC (mmol/L), determined by the broth microdilution method

Compound	*Candida albicans*		*Pseudomonas aeruginosa*		*Escherichia coli*		*Enterococcus faecalis*		*Staphylococcus aureus*		*Staphylococcus aureus* MRSA	
	ATCC 10231		ATCC 27853		ATCC 25922		ATCC 29212		ATCC 25923		clinical isolate	
	MIC	MBC	MIC	MBC	MIC	MBC	MIC	MBC	MIC	MBC	MIC	MBC
1	-[1]	-	$5.00^{a,A2}$	-	$5.00^{a,A}$	-	$5.00^{a,A}$	-	$5.00^{a,A}$	-	$5.00^{a,A}$	-
2	-	-	-	-	$5.00^{a,A}$	-	$2.50^{b,B}$	-	$0.62^{d,C}$	5.00^{a}	$2.50^{b,B}$	-
3	-	-	-	-	-	-	$5.00^{a,A}$	-	$5.00^{a,A}$	-	-	-
4	-	-	-	-	$5.00^{a,A}$	-	$5.00^{a,A}$	-	$5.00^{a,A}$	-	$5.00^{a,A}$	-
5	$1.25^{c,B}$	-	-	-	$5.00^{a,A}$	-	-	-	$5.00^{a,A}$	-	$5.00^{a,A}$	-
6	$0.16^{d,D}$	$0.31^{a,B}$	$5.00^{a,A}$	-	$2.50^{b,B}$	-	$2.50^{b,B}$	-	$1.25^{c,C}$	-	$0.08^{d,E}$	$2.50^{b,A}$
7												
8												
9	-	-	$5.00^{a,A}$	-	$5.00^{a,A}$	-	$2.50^{b,B}$	-	$1.25^{c,C}$	5.00^{a}	$2.50^{b,B}$	-
10	$5.00^{a,A}$	-	$5.00^{a,A}$	-	$5.00^{a,A}$	-	$5.00^{a,A}$	-	-	-	$5.00^{a,A}$	-
11	$5.00^{a,A}$	-	-	-	$5.00^{a,A}$	-	$5.00^{a,A}$	-	$5.00^{a,A}$	-	$5.00^{a,A}$	-
12	-	-	-	-	$5.00^{a,A}$	-	$5.00^{a,A}$	-	$2.50^{b,B}$	5.00^{a}	$5.00^{a,A}$	-
13	$2.50^{b,B}$	-	-	-	$5.00^{a,A}$	-	$5.00^{a,A}$	-	$2.50^{b,B}$	-	-	-
14	-	-	$5.00^{a,A}$	-	$5.00^{a,A}$	$5.00^{a,A}$	$2.50^{b,B}$	-	$1.25^{c,C}$	-	$1.25^{c,C}$	$5.00^{a,A}$
15	1.25c,C	-	-	-	5.00a,A	-	2.50b,B	-	2.50b,B	-	-	-
16	0.16d,B	0.31a,C	0.31b,A	5.00a,A	0.31c,A	5.00a,A	0.16c,B	5.00a,A	0.16e,B	2.50b,B	0.08d,C	2.50b,B
Amoxycillin			$0.07^{c,A}$	$0.14^{b,A}$	$0.02^{d,B}$	$0.07^{b,B}$	$0.001^{d,C}$	$0.01^{b,C}$	$0.001^{f,C}$	$0.004^{c,D}$		
Fluconazole	0.04^{e}	0.16^{b}										

As standard deviations do not exist, they are not presented in the table.

[1] Not achieved

[2] Values in the same column with different lowercase letters, as well as values in the same row with different capital letters are significantly different at $\alpha = 0.05$ (ANOVA, Tukey's HSD test).

3.8. Target fishing and molecular docking indicate possible antibacterial targets for BIPs

To indicate a possible mechanism of antimicrobial action of BIPs, similarity ensemble approach was applied [40]. In this method, the proteins are clustered according to the chemical similarity of their ligands, so chemical similarity of novel molecules with the ensemble of molecules from database gives a rational guess of potential cellular targets and possible pharmacology pathways. The three highest-ranked molecular targets for each of the most active ligands (compounds **6**, **10** and **16**) are shown in Table 6, while suggested molecular targets for other ligands are listed in Table S7.

Table 6. The three best-ranked molecular targets suggested by similarity ensemble search for compounds **6**, **10** and **16**. Overall rank is a combination of several parameters such as distance from the mean (*Z*-score) and Tanimoto similarity index (Max TC).

Compound	Suggested target	*Z*-score	Max TC
	Endothelin-converting enzyme 2	61.9499	0.3590
6	Cysteine protease falcipain-3	35.7526	0.4286
	Bacterial leucyl aminopeptidase	17.6778	0.3235
	Gag-Pro-Pol polyprotein	76.2021	0.3000
10	Endothelin-converting enzyme 2	56.1682	0.3256
	Bacterial leucyl aminopeptidase	21.9179	0.4000
	Amiloride-sensitive amine oxidase [copper-containing]	17.6168	0.2955
16	**Bacterial leucyl aminopeptidase**	17.1653	0.3143
	5'-AMP-activated protein kinase subunit gamma-1	15.7955	0.3171

As seen from Table 6, bacterial leucyl aminopeptidase is recognized as the best-ranked target for compounds **6, 10** and **16**. It is a Zn^{2+}-dependent protease that selectively cleaves amino-terminal Leu residue from polypeptides. These compounds showed notable activity against a panel of bacteria (Table 5), so it is reasonable to hypothesize this enzyme as a molecular target of BIPs in bacterial cells.

To characterize the possible molecular interactions between the most potent compound **16** and bacterial aminopeptidase we performed two molecular docking simulations. In the first one, no energy minimization/MD was performed upon removal of ligand so aminopeptidase binding pocket was in the exact conformation as in complex with the inhibitor 1-butaneboronic acid. In the second one, the protein side chains were minimized to remove steric bumps.

According to the lowest estimated free energy of binding (-7.71 *vs*. -7.42 kcal/mol), the complex of **16** in non-minimized protein structure (Fig. 5) is more stable compared to minimized one (Fig. S31). One pyridyl moiety resides deep into the binding pocket, forming the hydrophobic interactions with Met 180, Met 242, Phe 244, and Phe 248. Second pyridyl moiety is located at the entrance of binding pocket, forming hydrophobic interaction with Leu 155 and hydrogen bond with Gly 154 backbone. Two active site Zn^{2+} ions are coordinated to central pyridine N atom that occupies tetrahedral position where co-crystalized inhibitor was bound. The bridging Asp 117 is hydrogen bonded to azomethine N atom (Fig. 5).

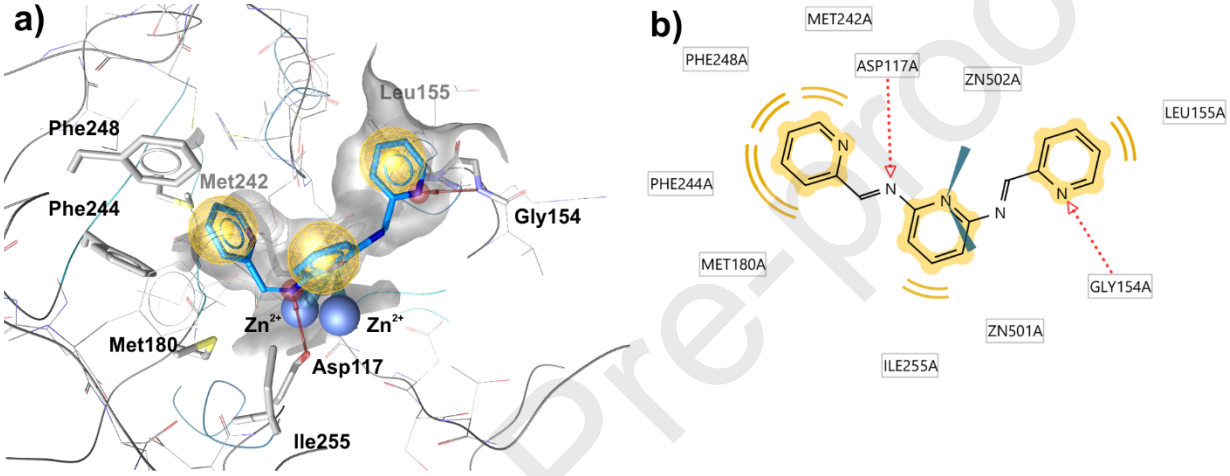

Fig. 5. a) Possible binding mode of **16** into the active site of Leu aminopeptidase (PDB code 1CP6); b) Ligand interaction diagram showing the most important interactions. The binding pocket of a receptor is shown as a transparent surface. The hydrophobic pharmacophores are shown as a yellow sphere, and hydrogen-bond acceptor pharmacophores are shown as red spheres. Hydrogen bonding interactions are depicted with red arrows, and zinc binding interactions are indicated with blue cones.

The qualitative SAR analysis reveals that the compounds having an additional coordinating atom near tridentate bis(imino)pyridine moiety are the most potent antibacterial BIPs. As target fishing analysis indicated Zn^{2+}-dependent Leu aminopeptidase as the most probable molecular target for the most potent BIPs, it is reasonable to hypothesize the metal chelating ability of BIPs as the main characteristics responsible for antibacterial activity.

4. Conclusion

In the present study, we reported synthesis, structural and biological characterization of a series of bis(imino)pyridines (BIPs). The formation of a stable, carbon-centered radical on a

pyridine ring is suggested by EPR spectroscopy and spin density derived from DFT calculations. Excellent antioxidant activity is found for several derivatives, while DFT calculations at ωB97XD/6-311++g(d,p) level aided the elucidation of the antioxidant mechanism. HAT is the main antioxidant mechanism for hydroxyl-substituted BIPs, while SET-PT governs the activity of other derivatives. The moderate inhibitory activity of BIPs toward AChE was found. The most potent compound **16** exert inhibition in the low micromolar range (IC_{50} = 20±4 μM), and binds to the peripheral anionic site of AChE as suggested by molecular docking. Moderate activity toward several bacterial and fungal strains is also confirmed. Similarity ensemble search combined with molecular docking suggested leucyl aminopeptidase as the plausible bacterial target for the most potent derivatives **6**, **10** and **16**.

Acknowledgements

The authors acknowledge financial support from Ministry of Education, Science and Technological development of Serbia, Ministry of Education, Science and Technological Development of Republic of Serbia, Contract number: 451-03-68/2020-14/200288, 451-03-68/2020-14/200026, and 451-03-68/2020-14/200135.

References

[1] Y.J. Wu, Heterocycles and Medicine. A Survey of the Heterocyclic Drugs Approved by the U.S. FDA from 2000 to Present., in: Prog. Heterocycl. Chem., 2012. https://doi.org/10.1016/B978-0-08-096807-0.00001-4.

[2] T.L.S. Kishbaugh, Pyridines and Imidazopyridines with Medicinal Significance, Curr. Top. Med. Chem. 16 (2016) 3274–3302. https://doi.org/http://dx.doi.org/10.2174/1568026616666160506145141.

[3] A.-Y. Guan, C.-L. Liu, X.-F. Sun, Y. Xie, M.-A. Wang, Discovery of pyridine-based agrochemicals by using Intermediate Derivatization Methods, Bioorg. Med. Chem. 24 (2016) 342–353. https://doi.org/10.1016/J.BMC.2015.09.031.

[4] S. Riaz, I.U. Khan, M. Bajda, M. Ashraf, Qurat-Ul-Ain, A. Shaukat, T.U. Rehman, S. Mutahir, S. Hussain, G. Mustafa, M. Yar, Pyridine sulfonamide as a small key organic molecule for the potential treatment of type-II diabetes mellitus and Alzheimer's disease: In vitro studies against yeast α-glucosidase, acetylcholinesterase and butyrylcholinesterase, Bioorg. Chem. 63 (2015) 64–71. https://doi.org/10.1016/j.bioorg.2015.09.008.

[5] R. Wang, Y. Chen, B. Yang, S. Yu, X. Zhao, C. Zhang, Design, synthesis, biological evaluation and molecular modeling of novel 1H-pyrrolo [2,3-b]pyridine derivatives as potential anti-tumor agents, Bioorg. Chem. 94 (2020) 103474. https://doi.org/10.1016/j.bioorg.2019.103474.

[6] E.H. Anouar, S. Raweh, I. Bayach, M. Taha, M.S. Baharudin, F. Di Meo, M.H. Hasan, A. Adam, N.H. Ismail, J.F.F. Weber, P. Trouillas, Antioxidant properties of phenolic Schiff bases: Structure-activity relationship and mechanism of action, J. Comput. Aided. Mol. Des. 27 (2013) 951–964. https://doi.org/10.1007/s10822-013-9692-0.

[7] H.F. Abd El-Halim, M.M. Omar, G.G. Mohamed, Synthesis, structural, thermal studies and biological activity of a tridentate Schiff base ligand and their transition metal complexes, Spectrochim. Acta - Part A Mol. Biomol. Spectrosc. 78 (2011) 36–44. https://doi.org/10.1016/j.saa.2010.06.003.

[8] C. Glotzbach, U. Kauscher, J. Voskuhl, N.S. Kehr, M.C.A. Stuart, R. Fröhlich, H.J. Galla, B.J. Ravoo, K. Nagura, S. Saito, S. Yamaguchi, E.U. Würthwein, Fluorescent modular boron systems based on NNN- and ONO-tridentate ligands: Self-assembly and cell imaging, J. Org. Chem. 78 (2013) 4410–4418. https://doi.org/10.1021/jo4003745.

[9] R.M. Wang, H.X. Feng, Y.F. He, C.G. Xia, Ji-Shuan Suo, Y.P. Wang, Preparation and catalysis of NaY-encapsulated Mn(III) Schiff-base complex in presence of molecular oxygen, J. Mol. Catal. A Chem. 151 (2000) 253–259. https://doi.org/10.1016/S1381-1169(99)00256-3.

[10] J. Devi, N. Batra, Synthesis, characterization and antimicrobial activities of mixed ligand transition metal complexes with isatin monohydrazone Schiff base ligands and heterocyclic nitrogen base, Spectrochim. Acta Part A Mol. Biomol. Spectrosc. 135 (2015) 710–719. https://doi.org/https://doi.org/10.1016/j.saa.2014.07.041.

[11] J. Devi, M. Yadav, D. Kumar, L.S. Naik, D.K. Jindal, Some divalent metal (II) complexes of salicylaldehyde-derived Schiff bases: Synthesis, spectroscopic characterization, antimicrobial and in vitro anticancer studies, Appl. Organomet. Chem. 33 (2019) e4693.

[12] A.A. Shanty, P.V. Mohanan, Heterocyclic Schiff bases as non toxic antioxidants: Solvent effect, structure activity relationship and mechanism of action, Spectrochim. Acta Part A Mol. Biomol. Spectrosc. 192 (2018) 181–187. https://doi.org/10.1016/J.SAA.2017.11.019.

[13] A. Paşahan, S. Köytepe, E. Ekinci, Synthesis, characterization of pyridine-based polyimides and their use as glucose oxidase immobilization media, E-Polymers. (2012) 1–10.

[14] I. Ahamad, R. Prasad, M.A. Quraishi, Thermodynamic, electrochemical and quantum chemical investigation of some Schiff bases as corrosion inhibitors for mild steel in hydrochloric acid solutions, Corros. Sci. 52 (2010) 933–942. https://doi.org/10.1016/j.corsci.2009.11.016.

[15] Z. Cimerman, N. Galic, B. Bosner, The Schiff bases of salicylaldehyde and aminopyridines as highly sensitive analytical reagents, Anal. Chim. Acta. 343 (1997) 145–153. https://doi.org/10.1016/S0003-2670(96)00587-9.

[16] S.B. Nimse, D. Pal, Free radicals, natural antioxidants, and their reaction mechanisms, RSC Adv. 5 (2015) 27986–28006. https://doi.org/10.1039/c4ra13315c.

[17] C.C. Winterbourn, Toxicity of iron and hydrogen peroxide: the Fenton reaction, Toxicol. Lett. 82–83 (1995) 969–974. https://doi.org/10.1016/0378-4274(95)03532-X.

[18] M.D. Milošević, N. Prlainović, M. Milčić, V. Nikolić, A. Božić, M. Bigović, A.D. Marinković, Solvent, structural, quantum chemical study and antioxidative activity of symmetrical 1-methyl-2,6-bis[2-(substituted phenyl)ethenyl]pyridinium iodides, J. Iran. Chem. Soc. 15 (2018) 2483–2501. https://doi.org/10.1007/s13738-018-1437-5.

[19] K. Murad, A. Deeb, F. Kandil, Synthesis, characterisation of some 2-azetidinone derivatives from 2,6-diaminopyridine and evaluation of their antimicrobial activity, Int. J.

ChemTech Res. 6 (2014) 3762–3766.
[20] N. Galić, D. Matković-Čalogović, Z. Cimerman, Structural characteristics of N,N′-bis(salicylidene)-2,6-pyridinediamine, J. Mol. Struct. 406 (1997) 153–158. https://doi.org/10.1016/S0022-2860(96)09608-1.
[21] K.R. Reddy, A. V. Raghu, H.M. Jeong, Siddaramaiah, Synthesis and characterization of pyridine-based polyurethanes, Des. Monomers Polym. 12 (2009) 109–118. https://doi.org/10.1163/156855509X412054.
[22] M. Misra, D. Das, K.B. Padhi, A.K. Panigrahi, A.K. Mohanty, Synthesis and characterization of a novel heterocyclic poly(Schiff base sulfide) polymer: Nucleophilic displacement polymerization of N,N′-bis(p-chloroben-zylidine)-2,6-diaminopyridine with sodium sulfide, J. Macromol. Sci. - Pure Appl. Chem. 35 (1998) 867–873. https://doi.org/10.1080/10601329808002017.
[23] K. Das, M. Dutta, B. Das, H.K. Srivastava, A. Kumar, Efficient Pincer-Ruthenium Catalysts for Kharasch Addition of Carbon Tetrachloride to Styrene, Adv. Synth. Catal. 361 (2019) 2965–2980. https://doi.org/10.1002/adsc.201900107.
[24] G.G. Mohamed, Synthesis, characterization and biological activity of bis(phenylimine) Schiff base ligands and their metal complexes, Spectrochim. Acta - Part A Mol. Biomol. Spectrosc. 64 (2006) 188–195. https://doi.org/10.1016/j.saa.2005.05.044.
[25] A.L. Vance, N.W. Alcock, J.A. Heppert, D.H. Busch, An Octahedral Template Based on a New Molecular Turn: Synthesis and Structure of a Model Complex and a Reactive, Diphenolic Ligand and Its Metal Complexes, Inorg. Chem. 37 (1998) 6912–6920. https://doi.org/10.1021/ic9714201.
[26] R. Rajesh, E.S. Sella, O. Blacque, K. Rajesh, Crystal structure of a new 2,6-bis(imino)pyridine derivative: (1 E,1′ E)-1,1′-(pyridine-2,6-diyl)bis[N -(4-chlorophenyl)ethan-1-imine], Acta Crystallogr. Sect. E Crystallogr. Commun. 75 (2019) 115–118. https://doi.org/10.1107/S2056989018017966.
[27] H.H. Hammud, A. Ghannoum, M.S. Masoud, Spectral regression and correlation coefficients of some benzaldimines and salicylaldimines in different solvents, Spectrochim. Acta Part A Mol. Biomol. Spectrosc. 63 (2006) 255–265. https://doi.org/10.1016/J.SAA.2005.04.020.
[28] J.M. Marković, N.P. Trišović, D. Mutavdžić, K. Radotić, I.O. Juranić, B.J. Drakulić, A.D. Marinković, Solvatochromism of symmetrical 2,6-distyrylpyridines. An experimental and theoretical study, Spectrochim. Acta - Part A Mol. Biomol. Spectrosc. 135 (2015) 435–446. https://doi.org/10.1016/j.saa.2014.07.023.
[29] T.A. Halgren, MMFF VI. MMFF94s option for energy minimization studies, J. Comput. Chem. 20 (1999) 720–729. https://doi.org/10.1002/(SICI)1096-987X(199905)20:7<720::AID-JCC7>3.0.CO;2-X.
[30] A. Pedretti, L. Villa, G. Vistoli, VEGA – An open platform to develop chemo-bio-informatics applications, using plug-in architecture and script programming, J. Comput. Aided. Mol. Des. 18 (2004) 167–173. https://doi.org/10.1023/B:JCAM.0000035186.90683.f2.
[31] M. Leopoldini, T. Marino, N. Russo, M. Toscano, Antioxidant Properties of Phenolic Compounds: H-Atom versus Electron Transfer Mechanism, J. Phys. Chem. A. 108 (2004) 4916–4922. https://doi.org/10.1021/jp037247d.
[32] E. Rezabal, J.M. Mercero, X. Lopez, J.M. Ugalde, A theoretical study of the principles regulating the specificity for Al(III) against Mg(II) in protein cavities, J. Inorg. Biochem.

101 (2007) 1192–1200. https://doi.org/10.1016/j.jinorgbio.2007.06.010.
[33] Z. Marković, J. Tošović, D. Milenković, S. Marković, Revisiting the solvation enthalpies and free energies of the proton and electron in various solvents, Comput. Theor. Chem. 1077 (2016) 11–17. https://doi.org/10.1016/j.comptc.2015.09.007.
[34] T. Lu, F. Chen, Multiwfn: A multifunctional wavefunction analyzer, J. Comput. Chem. 33 (2012) 580–592. https://doi.org/10.1002/jcc.22885.
[35] E.R. Johnson, S. Keinan, P. Mori-Sánchez, J. Contreras-García, A.J. Cohen, W. Yang, Revealing Noncovalent Interactions, J. Am. Chem. Soc. 132 (2010) 6498–6506. https://doi.org/10.1021/ja100936w.
[36] W. Humphrey, A. Dalke, K. Schulten, VMD: Visual molecular dynamics, J. Mol. Graph. 14 (1996) 33–38. https://doi.org/10.1016/0263-7855(96)00018-5.
[37] M.J. Frisch, G.W. Trucks, H.B. Schlegel, G.E. Scuseria, M.A. Robb, J.R. Cheeseman, G.. Scalmani, V. Barone, G.A. Petersson, H. Nakatsuji, X. Li, M. Caricato, A.V. Marenich, J. Bloino, B.G. Janesko, R. Gomperts, B. Mennucci, H.P. Hratchian, J.V. Ortiz, J.L. Izmaylov, A. F; Sonnenberg, D. Williams-Young, F. Ding, F. Lipparini, F. Egidi, J. Goings, B. Peng, A. Petrone, T. Henderson, D. Ranasinghe, V.G. Zakrzewski, J. Gao, N. Rega, G. Zheng, W. Liang, M. Hada, M. Ehara, K. Toyota, R. Fukuda, J. Hasegawa, M. Ishida, T. Nakajima, Y. Honda, O. Kitao, H. Nakai, T. Vreven, J.. Throssell, K; Montgomery, J. A, J.E. Peralta, F. Ogliaro, M.J. Bearpark, J.J. Heyd, E.N. Brothers, K.N. Kudin, V.N. Staroverov, T.A. Keith, R. Kobayashi, J. Normand, K. Raghavachari, A.P. Rendell, J.C. Burant, S.S. Iyengar, J. Tomasi, M. Cossi, J.M. Millam, M. Klene, C. Adamo, R. Cammi, J.W. Ochterski, R.L. Martin, K. Morokuma, O. Farkas, J.B. Foresman, D.J. Fox, Gaussian 16, version B.01, Gaussian, Inc, Wallingford CT, (2016).
[38] Y. Bourne, H.C. Kolb, Z. Radić, K.B. Sharpless, P. Taylor, P. Marchot, Freeze-frame inhibitor captures acetylcholinesterase in a unique conformation, Proc. Natl. Acad. Sci. U. S. A. 101 (2004) 1449 LP – 1454. https://doi.org/10.1073/pnas.0308206100.
[39] O. Trott, A.J. Olson, AutoDock Vina: improving the speed and accuracy of docking with a new scoring function, efficient optimization, and multithreading., J. Comput. Chem. 31 (2010) 455–61. https://doi.org/10.1002/jcc.21334.
[40] M.J. Keiser, B.L. Roth, B.N. Armbruster, P. Ernsberger, J.J. Irwin, B.K. Shoichet, Relating protein pharmacology by ligand chemistry, Nat. Biotechnol. 25 (2007) 197–206. https://doi.org/10.1038/nbt1284.
[41] C.C. De Paola, B. Bennett, R.C. Holz, D. Ringe, G.A. Petsko, 1-Butaneboronic Acid Binding to Aeromonas proteolytica Aminopeptidase: A Case of Arrested Development, Biochemistry. 38 (1999) 9048–9053. https://doi.org/10.1021/bi9900572.
[42] C.R. Søndergaard, M.H.M. Olsson, M. Rostkowski, J.H. Jensen, Improved treatment of ligands and coupling effects in empirical calculation and rationalization of pKa values, J. Chem. Theory Comput. 7 (2011) 2284–2295.
[43] J.C. Phillips, R. Braun, W. Wang, J. Gumbart, E. Tajkhorshid, E. Villa, C. Chipot, R.D. Skeel, L. Kalé, K. Schulten, Scalable Molecular Dynamics with NAMD, J. Comput. Chem. 26 (2005) 1781–1802. https://doi.org/10.1002/jcc.20289.
[44] D. Santos-Martins, S. Forli, M.J. Ramos, A.J. Olson, AutoDock4(Zn): an improved AutoDock force field for small-molecule docking to zinc metalloproteins., J. Chem. Inf. Model. 54 (2014) 2371–9. https://doi.org/10.1021/ci500209e.
[45] M.F. Sanner, Python: a programming language for software integration and development., J. Mol. Graph. Model. 17 (1999) 57–61.

[46] G.M. Morris, R. Huey, W. Lindstrom, M.F. Sanner, R.K. Belew, D.S. Goodsell, A.J. Olson, AutoDock4 and AutoDockTools4: Automated docking with selective receptor flexibility., J. Comput. Chem. 30 (2009) 2785–2791. https://doi.org/10.1002/jcc.21256.
[47] G. Wolber, T. Langer, LigandScout: 3-D pharmacophores derived from protein-bound ligands and their use as virtual screening filters., J. Chem. Inf. Model. 45 (2005) 160–169. https://doi.org/10.1021/ci049885e.
[48] P. Dohare, M.A. Quraishi, I.B. Obot, A combined electrochemical and theoretical study of pyridine-based Schiff bases as novel corrosion inhibitors for mild steel in hydrochloric acid medium, J. Chem. Sci. 130 (2018) 1–19. https://doi.org/10.1007/s12039-017-1408-x.
[49] J. Pei, C.C. Hsu, R. Zhang, Y. Wang, K. Yu, G. Huang, Unexpected Reduction of Iminoquinone and Quinone Derivatives in Positive Electrospray Ionization Mass Spectrometry and Possible Mechanism Exploration, J. Am. Soc. Mass Spectrom. 28 (2017) 2454–2461. https://doi.org/10.1007/s13361-017-1770-4.
[50] R. De Vreese, K. Muylaert, C. Maton, L. Dereu, F. Taillieu, T. Harth, R. Van Deun, H. Vrielinck, C. V. Stevens, M. D'hooghe, Synthesis of bis-8-hydroxyquinolines via an imination or a Suzuki-Miyaura coupling approach, Tetrahedron Lett. 58 (2017) 3803–3807. https://doi.org/10.1016/j.tetlet.2017.08.039.
[51] M.O. Puskullu, B.T. and S. Suzen, Recent Studies of Antioxidant Quinoline Derivatives, Mini-Reviews Med. Chem. 13 (2013) 365–372. https://doi.org/http://dx.doi.org/10.2174/1389557511313030005.
[52] J. Devi, J. Yadav, N. Singh, Synthesis, characterisation, in vitro antimicrobial, antioxidant and anti-inflammatory activities of diorganotin(IV) complexes derived from salicylaldehyde Schiff bases, Res. Chem. Intermed. 45 (2019) 3943–3968. https://doi.org/10.1007/s11164-019-03830-3.
[53] M.N. Alam, N.J. Bristi, M. Rafiquzzaman, Review on in vivo and in vitro methods evaluation of antioxidant activity, Saudi Pharm. J. 21 (2013) 143–152. https://doi.org/10.1016/j.jsps.2012.05.002.
[54] Z. Xu, B. Lu, Q. Xiang, Y. Li, S. Li, Y. Lin, J. Pang, Radical-scavenging activities of marine-derived xyloketals and related chromanes, Acta Pharm. Sin. B. 3 (2013) 322–327. https://doi.org/10.1016/j.apsb.2013.06.008.
[55] E. Espinosa, E. Molins, C. Lecomte, Hydrogen bond strengths revealed by topological analyses of experimentally observed electron densities, Chem. Phys. Lett. (1998). https://doi.org/10.1016/S0009-2614(98)00036-0.
[56] R. Parthasarathi, V. Subramanian, N. Sathyamurthy, Hydrogen Bonding in Phenol, Water, and Phenol−Water Clusters, J. Phys. Chem. A. 109 (2005) 843–850. https://doi.org/10.1021/jp046499r.
[57] M. Saqib, S. Iqbal, A. Mahmood, R. Akram, Theoretical Investigation for Exploring the Antioxidant Potential of Chlorogenic Acid: A Density Functional Theory Study, Int. J. Food Prop. 19 (2016) 745–751. https://doi.org/10.1080/10942912.2015.1042588.
[58] J.S. Wright, E.R. Johnson, G.A. DiLabio, Predicting the activity of phenolic antioxidants: Theoretical method, analysis of substituent effects, and application to major families of antioxidants, J. Am. Chem. Soc. 123 (2001) 1173–1183. https://doi.org/10.1021/ja002455u.
[59] G.. DiLabio, D.. Pratt, J.. Wright, Theoretical calculation of gas-phase ionization potentials for mono- and polysubstituted benzenes, Chem. Phys. Lett. 311 (1999) 215–220. https://doi.org/10.1016/S0009-2614(99)00786-1.

[60] Y. Bourne, P. Taylor, Z. Radić, P. Marchot, Structural insights into ligand interactions at the acetylcholinesterase peripheral anionic site, EMBO J. 22 (2003) 1–12. https://doi.org/10.1093/emboj/cdg005.

Declaration of interests

☒ The authors declare that they have no known competing financial interests or personal relationships that could have appeared to influence the work reported in this paper.

☐The authors declare the following financial interests/personal relationships which may be considered as potential competing interests:

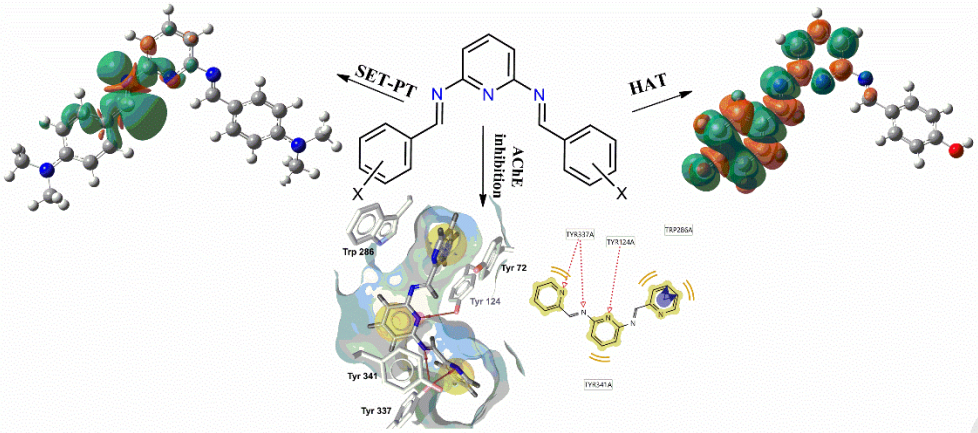

Highlights

- Bis(imino)pyridines (BIPs) are potent antioxidants in DPPH, ABTS and CUPRAC assay
- HAT governs antioxidant activity of OH-BIPs, while SET-PT dominates for other BIPs
- BIPs form a stable, carbon-centered radical cation in a solution
- Docking studies rationalized anticholinesterase and antimicrobial activity of BIPs